Electronic Supplementary Information

Materials

1-Pyrenecarboxylic acid (97 %) was purchased from Meryer Co. Ltd. (Shanghai). 1-Pyrenebutyric acid (95%), octafluoronaphthalene (96 %), L-alanine methyl ester hydrochloride (98 %), D-alanine methyl ester hydrochloride (98 %) and *tert*-Butyl (3-aminopropyl) carbamate (97%) were purchased from Bide Pharmatech Co., Ltd. (Shanghai). Trifluoroacetic acid (TFA, AR) was purchased from Innochem (Beijing). All solvents were purchased from FuYu Chemical Reagent Co. Ltd. (Tianjin). Both chemicals and solvents were used without further purification. Water is deionized (DI) water.

Characterizations

^{1}H NMR, ^{19}F NMR, ^{13}C NMR, NOESY (nuclear overhauser effect spectroscopy) and DOSY (diffusion ordered spectroscopy) spectra to characterize molecular structures were measured on a Bruker AVANCE III HD 400 MHz spectrometer (Switzerland) at room temperature with tetramethylsilane (TMS) as reference. Dimethyl sulfoxide-d (DMSO-d_6) and $CDCl_3$ were used. Concentration-dependent ^{1}H NMR in DMSO-d_6 were recorded *via* 600 MHz NMR spectrometer (JEOL ECZ600R/S3). High-resolution mass spectrometry (HR-MS) was performed via an Agilent Q-TOF 6510 MS spectrometer (America). UV-Vis spectra were recorded via UV-1900 from SHIMADZU (Japan). Fluorescence and temperature-variation fluorescence spectra were measured by FluoroMax-4 from Horiba (Japan). Circular dichroism (CD) spectra were measured with Applied Photophysics Chirascan V100 (England). Transmission electron microscope (TEM) images were measured by a HITACHI JEM-100CX II electron microscope (Japan). The samples for TEM detection were dropped in the copper grid and air-dried. Atomic force microscopy (AFM) images were recorded by Bioscope Resolve from Bruker (America) with tapping contact mode. The AFM sample was dropped on the mica wafer and dried at room temperature. Powder X-ray diffraction (XRD) patterns were collected on a Rigaku SmartLab 9KW X-ray diffraction (Japan) with Cu Kα radiation (λ = 0.15406 nm, voltage 45 KV, current 200

mA, power 9 KW). The samples were casted onto cover slide glasses (18 mm × 18 mm) and dried to form thin films. The average diameter of aggregation was recorded by DLS measurement with NanoZS of Malvern Panalytical (UK).

Preparation of aggregates

For $CHCl_3$/MCH system, we dissolved PMA or PBA in $CHCl_3$ to prepare concentrated stock solution of 5 mM. Aggregates were prepared through adding 200 μL solution to a screw-neck glass vial *via* pipette and 800 μL MCH was immediately added. The total concentration of sample was 1 mM in the mixture of $CHCl_3$/MCH. We tightened the vial to minimize solvent volatilization. For DMSO/H_2O system, powder of PMA or PBA was dissolved in DMSO with concentration of 50 mM. We attained 30 μL solution *via* adding 20 μL concentrated solution and 10 μL DMSO into a screw-neck glass. Sample was prepared by further adding 970 μL H_2O to the above solution. The total concentration of sample was 1 mM in the mixture of DMSO/H_2O. And before characterization, samples were incubated for 12 h at room temperature. We did not consider the small amount of volatilization that may occur during samples aging process. The properties of CD spectra, morphology (TEM and AFM images) and XRD pattern are all repeatable with different batch samples.

Synthesis

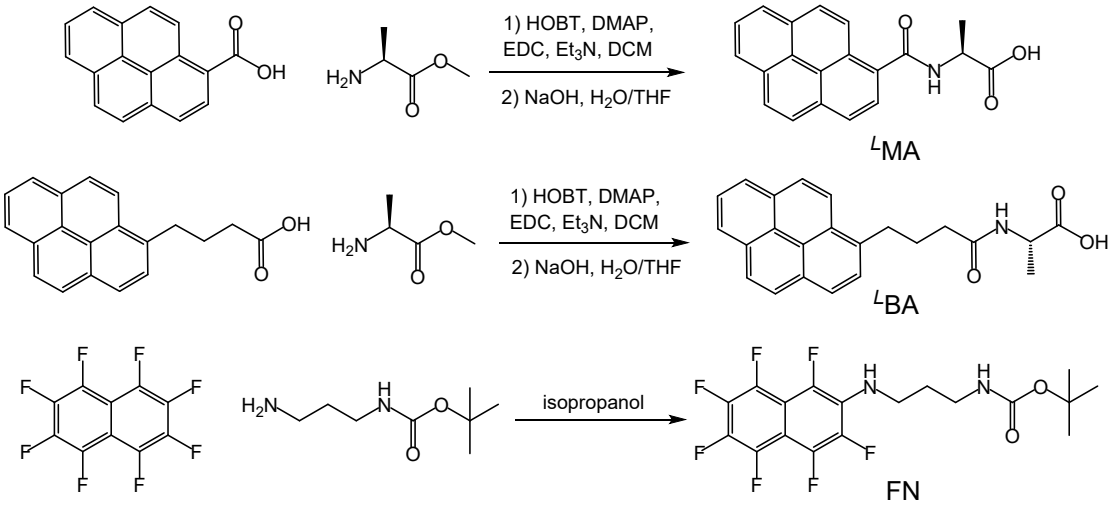

Scheme S1. The synthesis process of ^{L}MA, ^{L}BA and PN.

^{L}MA and ^{L}BA were prepared via condensation reaction. In details, 1-pyrenecarboxylic acid (1.7 g, 7 mmol) was mixed with L-alanine methyl ester hydrochloride (2 g, 10

mmol) in dichloromethane (DCM, 50 mL). 1-(3-dimethylaminopropyl)-3-ethylcarbodiimide (EDC, 2 g, 10 mmol), 1-hydroxybenzotriazole (HOBT, 135 mg, 1 mmol), 4-dimethylaminopyridine (DMAP, 122 mg, 1 mmol) and triethylamine (Et_3N, 2 mL) were added into the mixture. After 12 h reaction at room temperature, crude products were washed by saturated sodium chloride (NaCl) aqueous solution. The DCM phase was dried with anhydrous sodium sulfate (Na_2SO_4), and evaporated solvent via rotary evaporator. Column chromatography was used to purify crude produce (ethyl acetate: petroleum ether = 1:3). The obtained white powder was dissolved via tetrahydrofuran (THF, 20 mL). Sodium hydroxide (NaOH, 1 g, 25 mmol) and water (20 mL) mixed with the solution, which was stirred at room temperature for 1 h. Hydrochloric acid was used adjusting the solution to acidity. The mixture was extracted by DCM and dried with anhydrous Na_2SO_4. ^{L}MA powder was obtained by evaporating solvent. Yield: 67 %. ^{1}H NMR (400 MHz, DMSO-d_6, 298 K) δ = 12.69 (s, 1H), 9.03 (d, 1 H), 8.59 (d, 1H), 8.37-8.34 (m, 3H), 8.28-8.22 (m, 3H), 8.16-8.11 (m, 2H), 4.62-4.55 (m, 1H), 1.47 (d, 3H). ^{13}C NMR (101 MHz, DMSO-d_6) δ 174.83, 169.42, 132.10, 131.20, 130.72, 128.79, 128.54, 128.40, 127.71, 127.06, 126.28, 126.10, 125.83, 125.29, 124.85, 124.24, 124.12, 67.48, 48.88, 25.58, 17.32. HRMS (TOF) m/z $[M+H]^+$, calcd for $C_{20}H_{15}NO_3$, 317.1052; found, 318.1109.

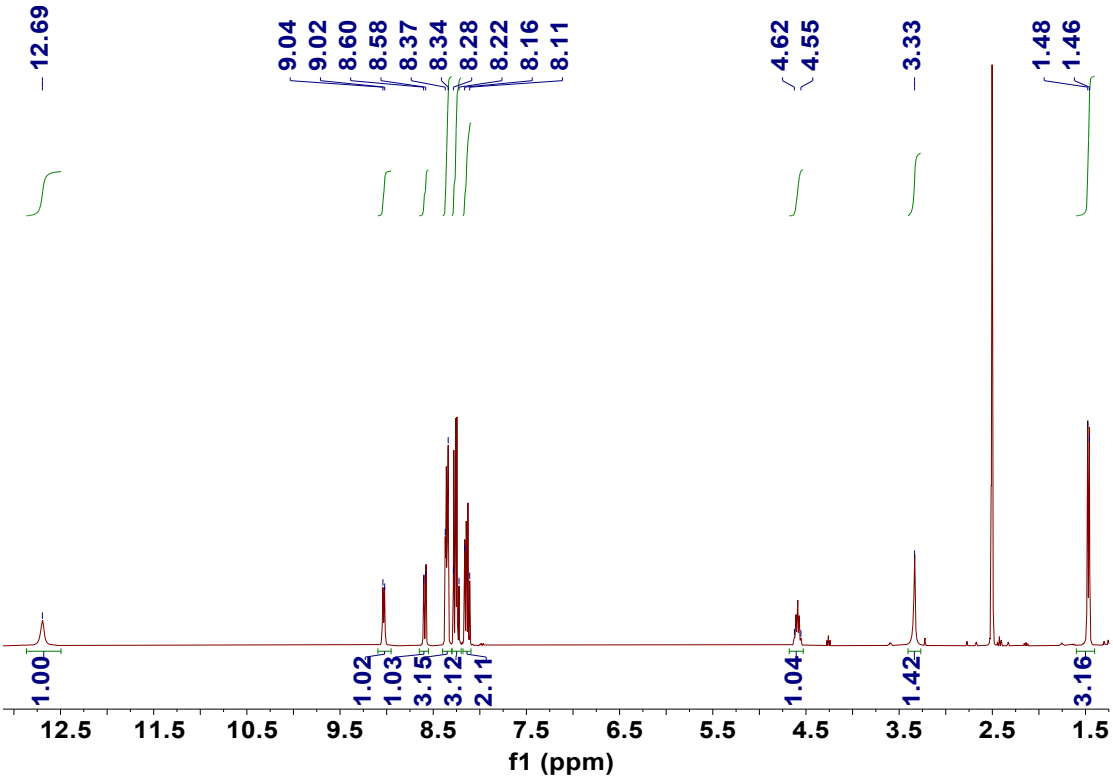

Figure S1. ^{1}H NMR of ^{L}MA

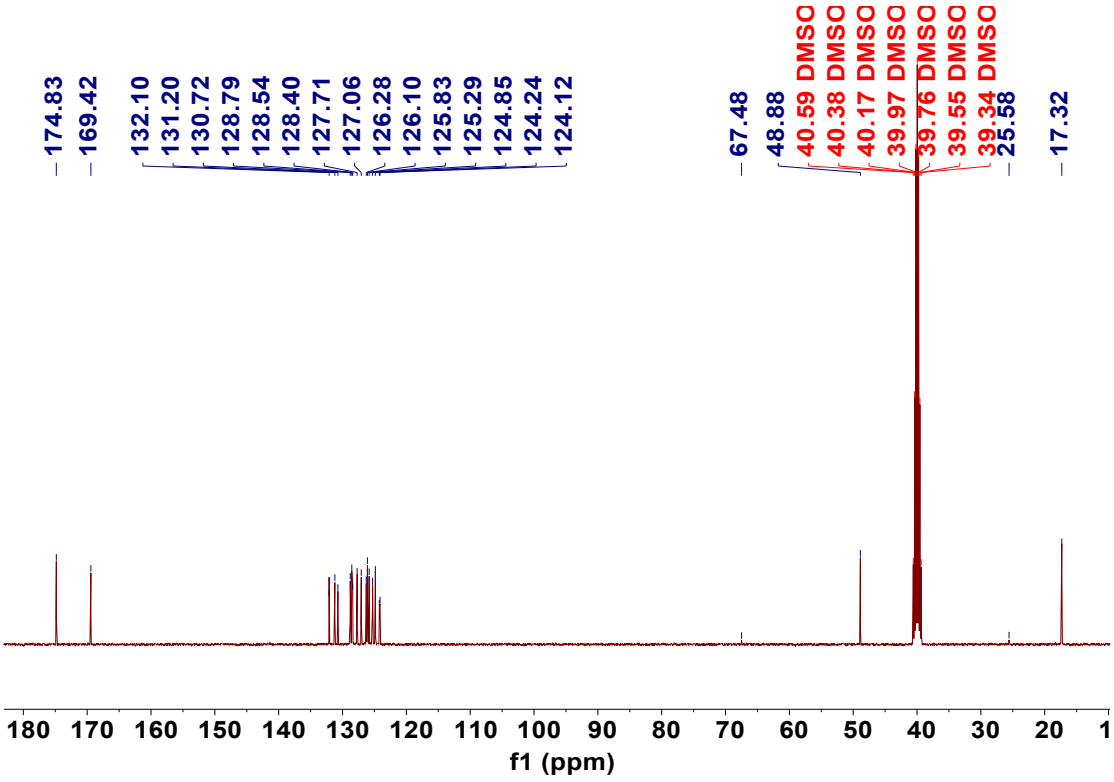

Figure S2. ^{13}C NMR of ^{L}MA

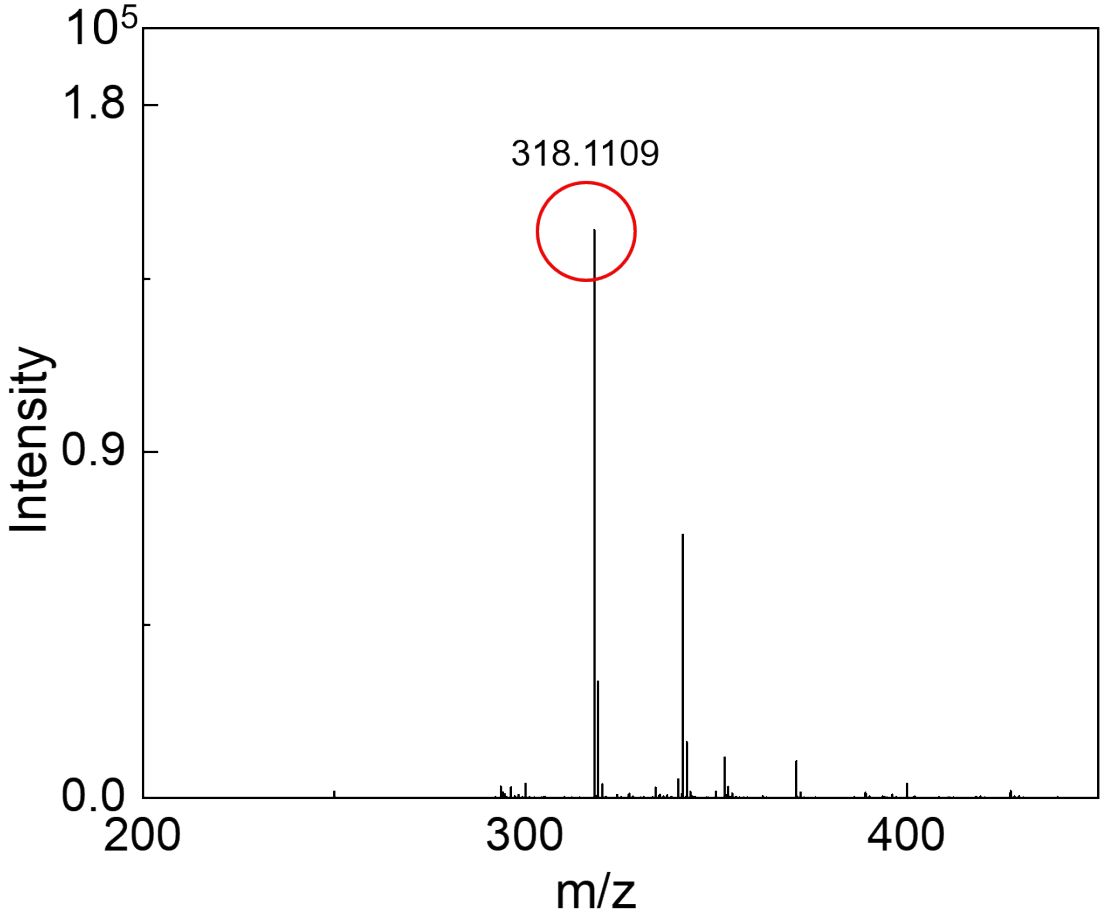

Figure S3. HRMS (TOF) of ^{L}MA

^{L}BA was prepared via the similar method. Pyrene-1-butyric acid (1.7 g, 6 mmol) was mixed with L-alanine methyl ester hydrochloride diethylmalonate (2 g, 10 mmol), EDC (2 g, 10 mmol), HOBT (135 mg, 1 mmol), DMAP (122 mg, 1 mmol) and Et_3N (2 mL) in DCM. After 12 h reaction at room temperature, crude products were washed by saturated NaCl aqueous solution and dried via anhydrous Na_2SO_4, which was subjected to column purification to obtain product. Hydrolysis reaction was occurred in LiOH (1 g, 25 mM) with THF (20 mL), water (20 mL) at room temperature for 1 h. Hydrochloric acid was used adjusting the solution to acidity. The mixture was extracted by DCM and dried with anhydrous Na_2SO_4. ^{L}MA powder was obtained by evaporating solvent. Yield: 79 %. ^{1}H NMR (400 MHz, DMSO-d_6, 298 K) δ = 12.39 (s, 1H), 8.40 (d, 1 H), 8.28 (t, 2H), 8.21 (m, 3H), 8.14 (m, 2H), 8.07 (t, 1H), 7.96 (d, 1H), 4.24 (t, 1H), 3.32 (m, 5 H, β-H mixed with H_2O-H from DMSO-d_6), 2.29 (m, 2H), 2.01 (m, 2H), 1.27 (d, 3H). ^{13}C NMR (101 MHz, DMSO-d_6) δ 175.05, 172.32, 137.14, 131.37, 130.92, 129.78,

128.99, 128.07,127.95, 127.71, 126.98, 126.62, 125.44, 125.27, 124.71, 124.06, 47.92, 35.14, 32.62, 28.03, 17.58. HRMS (TOF) m/z $[M+H]^+$, calcd for $C_{23}H_{21}NO_3$, 359.1521; found, 360.1575.

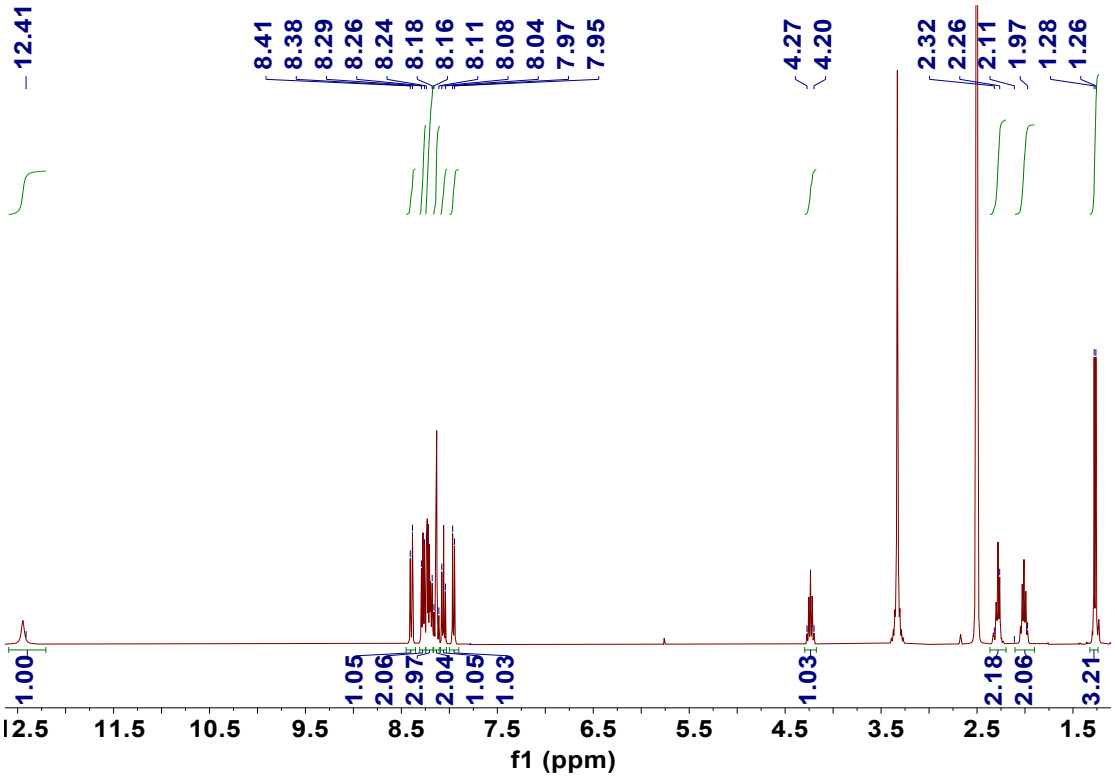

Figure S4. ^{1}H NMR of ^{L}BA

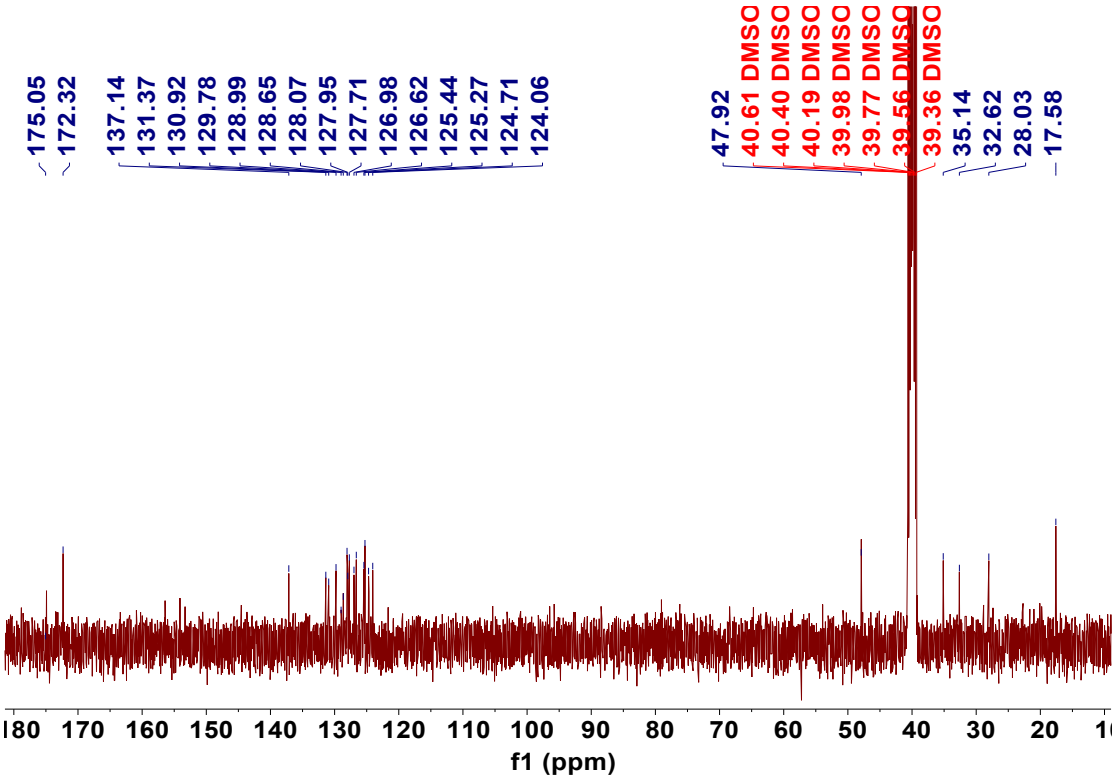

Figure S5. ^{13}C NMR of ^{L}BA

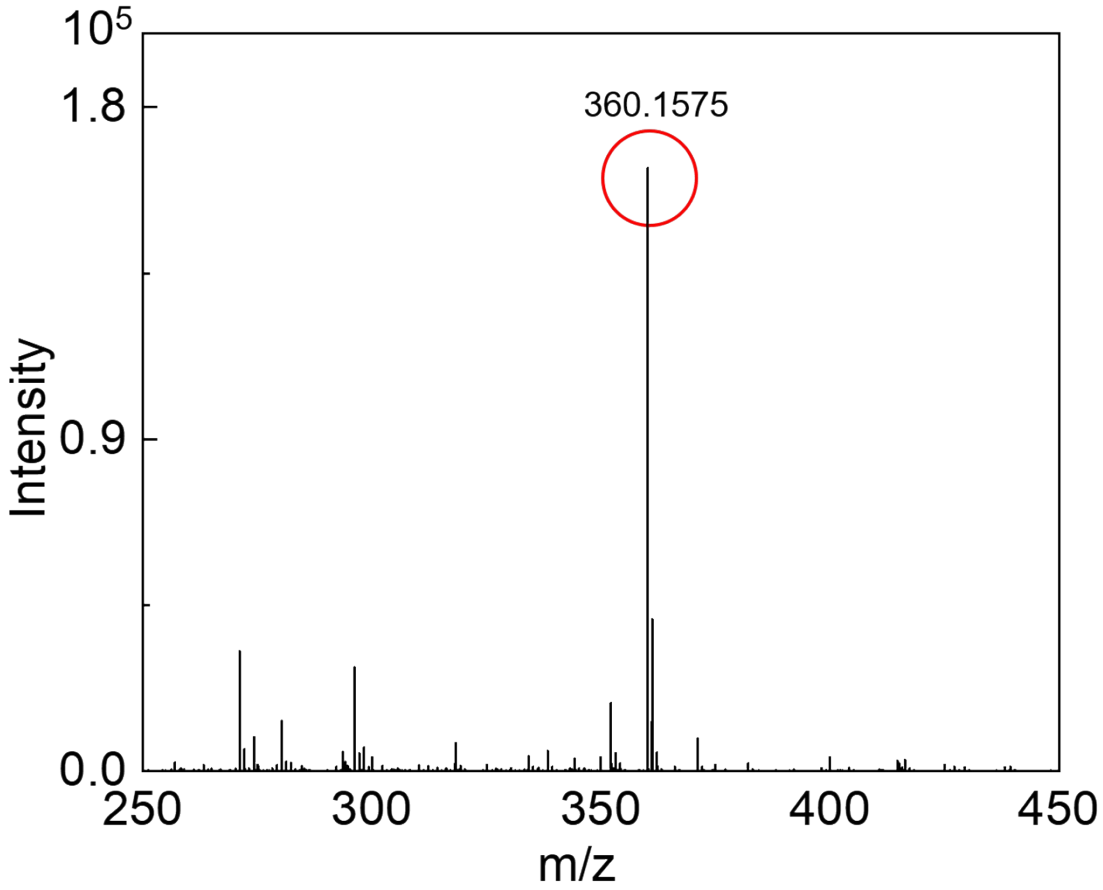

Figure S6. HRMS (TOF) of ^{L}BA

FN was synthesis via octoflonaphthalene (OFN) and N-boc-1,3-diaminopropane. OFN (2.7 g, 10 mmol) was dissolved with isopropanol. Excess N-boc-1,3-diaminopropane (2 mL) was added to the solution. The mixture was stirred at room temperature for a week. After evaporating solvent, the crude product was subjected to column purification (DCM) to obtain purity product 1.50 g. Yield: 35 %. ^{1}H NMR (400 MHz, $CDCl_3$, 298 K) δ = 4.6 (s, 2H), 3.54 (m, 2 H), 3.27 (m, 2H), 1.78 (m, 2H), 1.46 (s, 6H). ^{19}F NMR (376 MHz, $CDCl_3$, 298 K) δ = 144.60 (d, 1F), 147.62 (m, 1F), 148.63 (m, 1F), 149.62 (s, 2F), 156.96 (s, 1F), 150.99 (s, 1F). ^{13}C NMR (101 MHz, DMSO-d_6) δ 156.19, 142.27, 139.79, 139.26, 137.32, 136.89, 127.62, 127.50, 127.37, 108.22, 100.99, 77.97, 42.59, 42.53, 37.51, 30.99, 28.63. HRMS (TOF) m/z $[M+H]^+$, calcd for $C_{18}H_{17}F_7N_2O_2$, 426.1178; found, 427.1230.

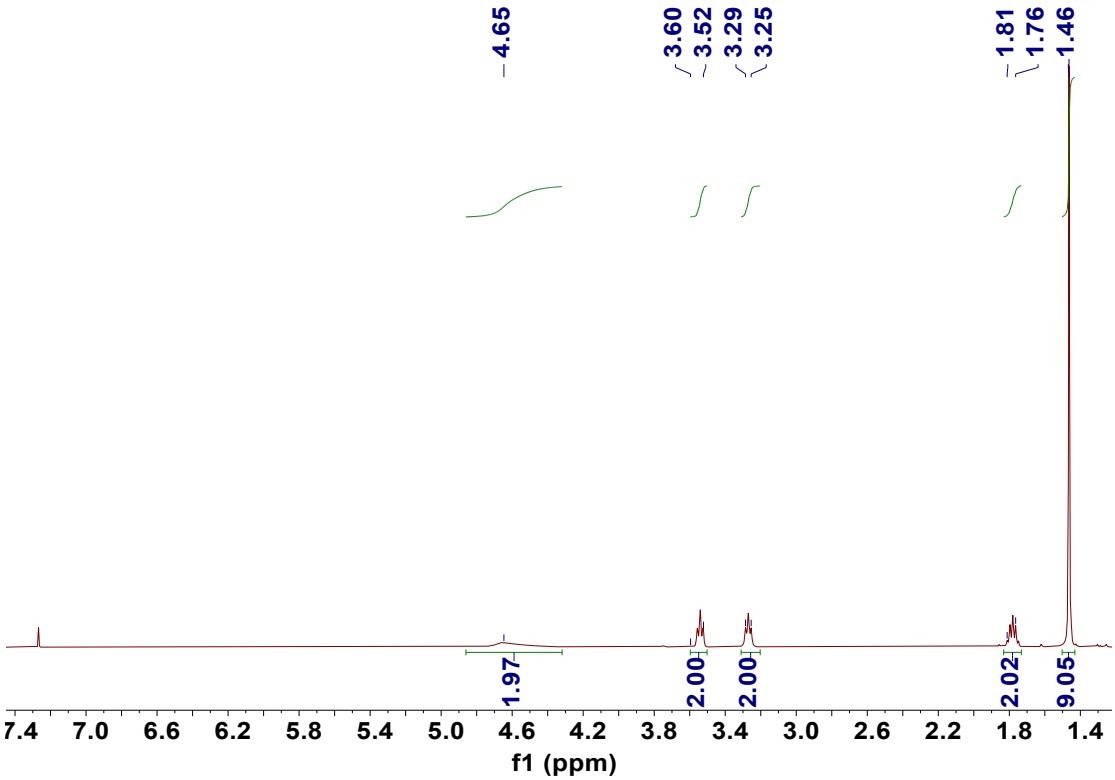

Figure S7. ^{1}H NMR of FN

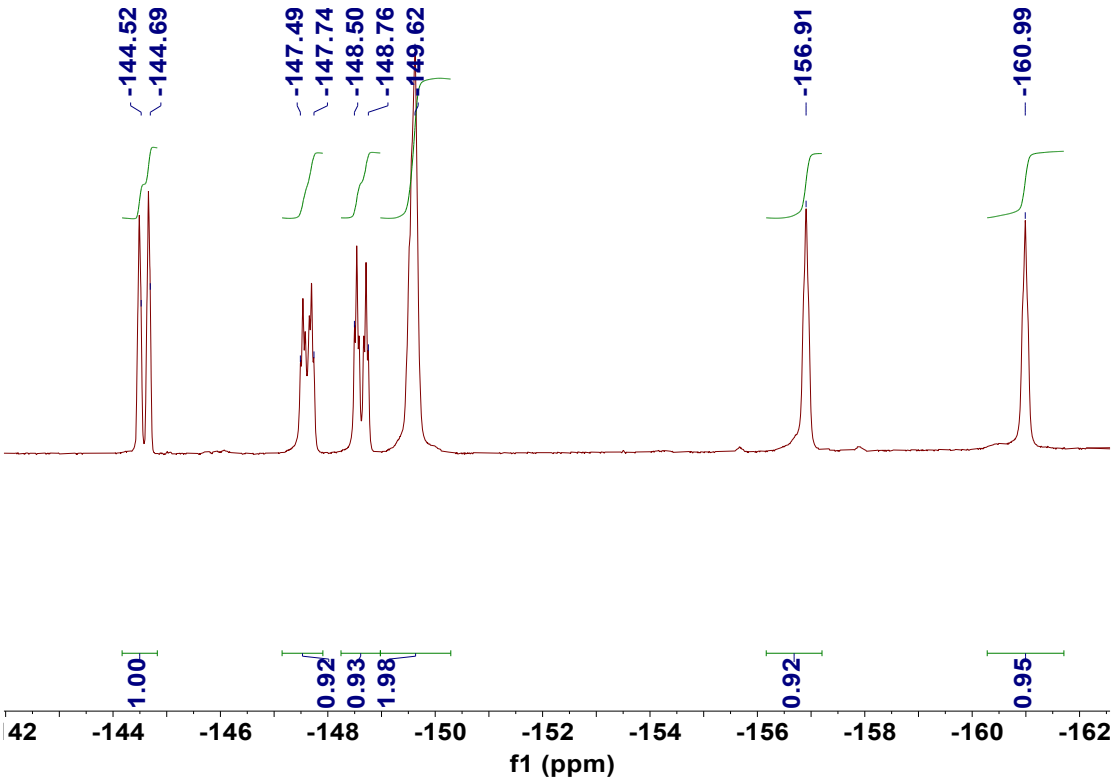

Figure S8. ^{19}F NMR of FN

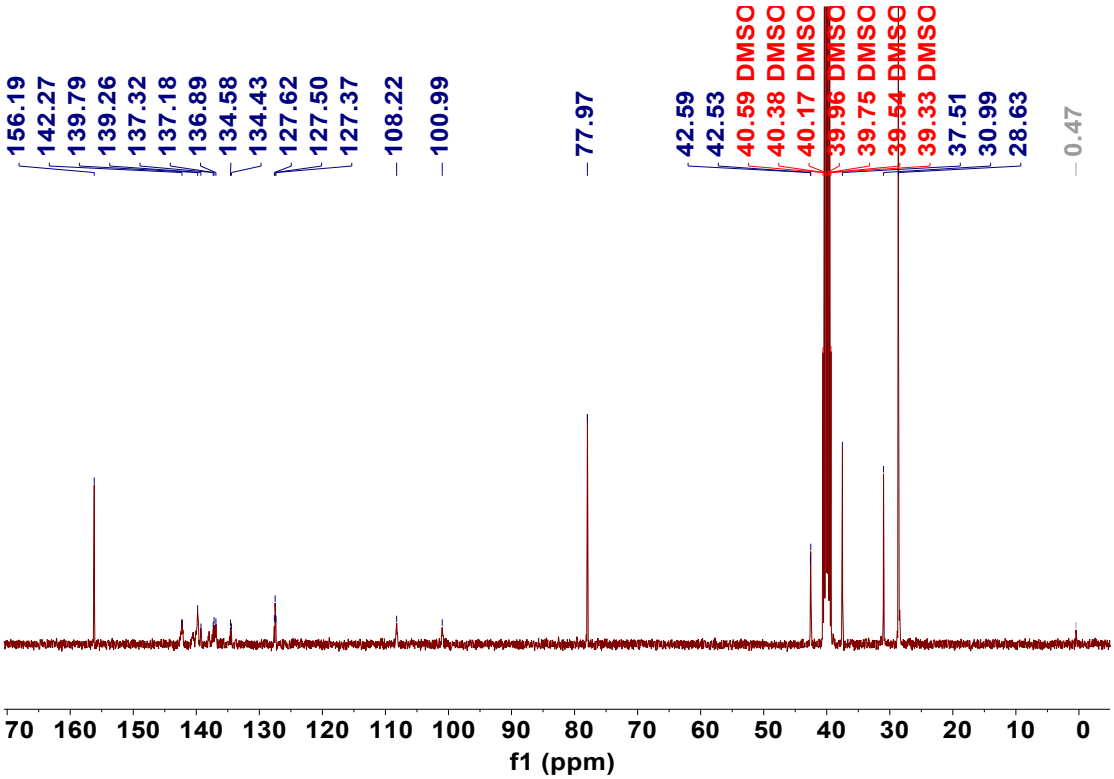

Figure S9. ^{13}C NMR of ^{L}FN

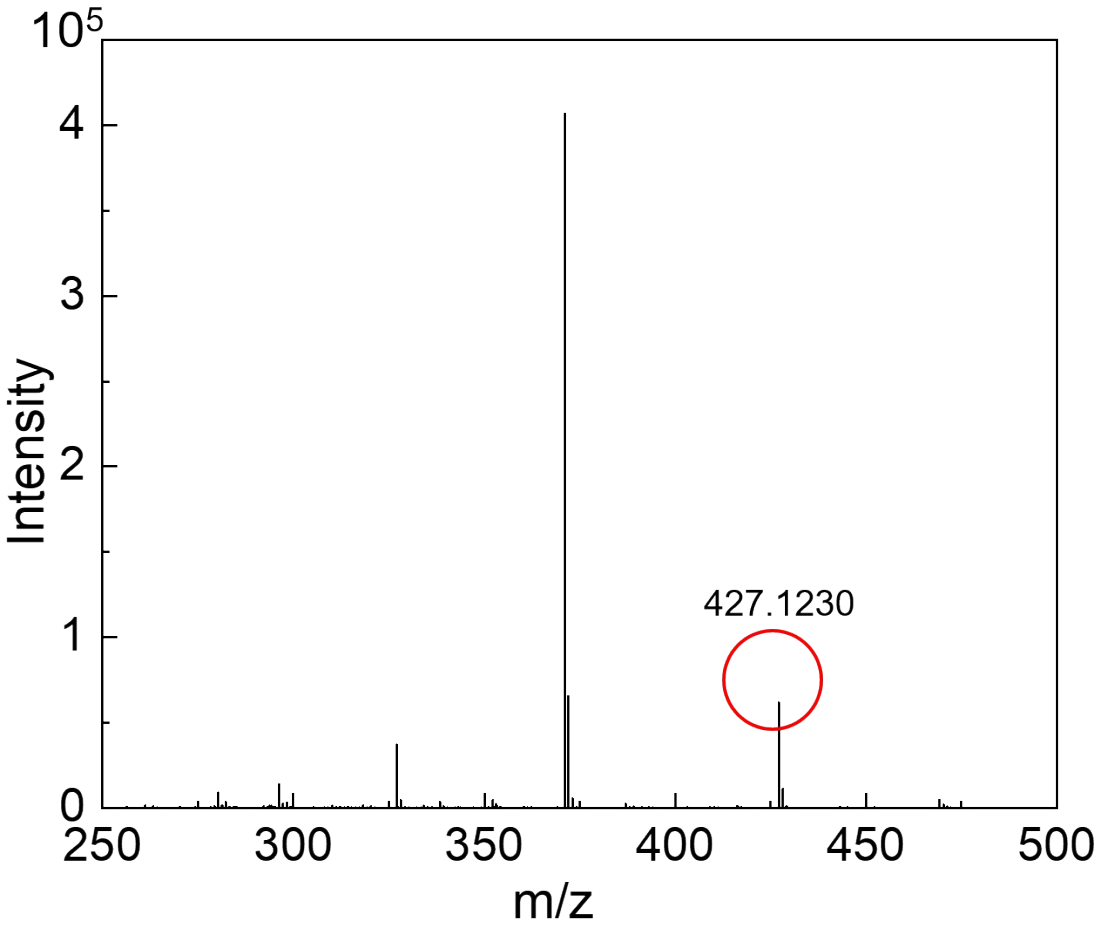

Figure S10. HRMS (TOF) of ^{L}FN

Preparation of compound PMA and PBA

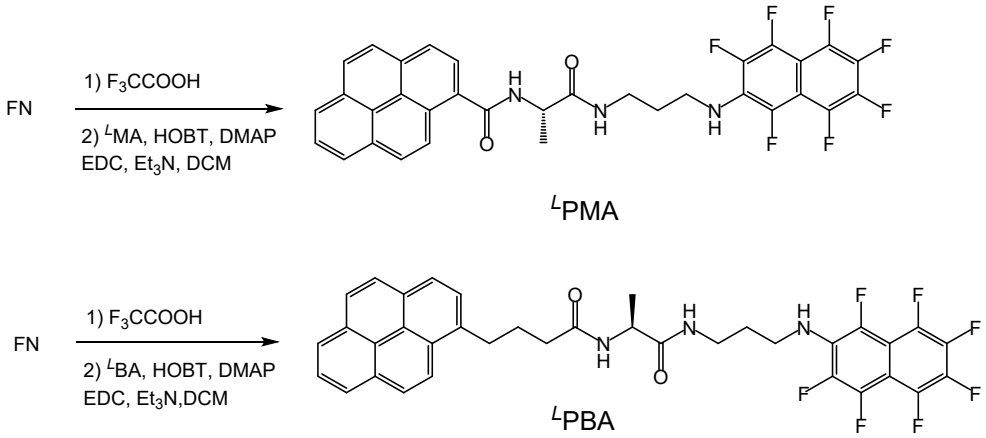

Scheme S2. Preparation of ^{L}PMA and ^{L}PBA.

FN (852 mg, 2 mM) was mixed with TFA 5 mL) for ten minutes to deprotect boc. After evaporated solvent, ^{L}MA (476 mg, 1.5 mM), HOBT (27 mg, 0.2 mM), DMAP (24 mg, 0.2 mM), EDC (400 mg, 2 mM), Et_3N (1 mL) and DCM (40 mL) as solvent were added.

The mixture was stirred at room temperature for 12 h. After evaporating solvent, the crude product was subjected to column purification to obtain pure product 0.65 g. Yield: 69 %. ^{1}H NMR (400 MHz, DMSO-d_6, 298 K) δ 8.81 (d, 1H), 8.56 (d, 1H), 8.31 (m, 3H), 8.24 (m, 2H), 8.17 (m, 2H), 8.10 (m, 2H), 6.25 (s, 1H), 4.58 (m, 1H), 3.47 (m, 2H), 3.25 (m, 2H), 1.79 (m, 2H), 1.40 (d, 3H). ^{19}F NMR (376 MHz, DMSO-d_6, 298 K) δ -145.50 (m, 1F), -148.39 (s, 1F), -148.81 (m, 1F), -149.84 (m, 1F), -150.97 (m, 1F), -157.79 (m, 1H), -162.69 (t, 1F). ^{13}C NMR (101 MHz, DMSO-d_6) δ 173.20, 169.18, 132.08, 131.74, 131.10, 130.58, 128.69, 128.39, 128.26, 127.62, 126.93, 126.15, 125.98, 125.93, 125.28, 124.66, 124.10, 123.95, 49.93, 42.63, 36.34, 30.65, 18.24. HRMS (TOF) m/z $[M+H]^+$, calcd for $C_{33}H_{22}F_7N_3O_2$, 625.1600; found, 626.1699.

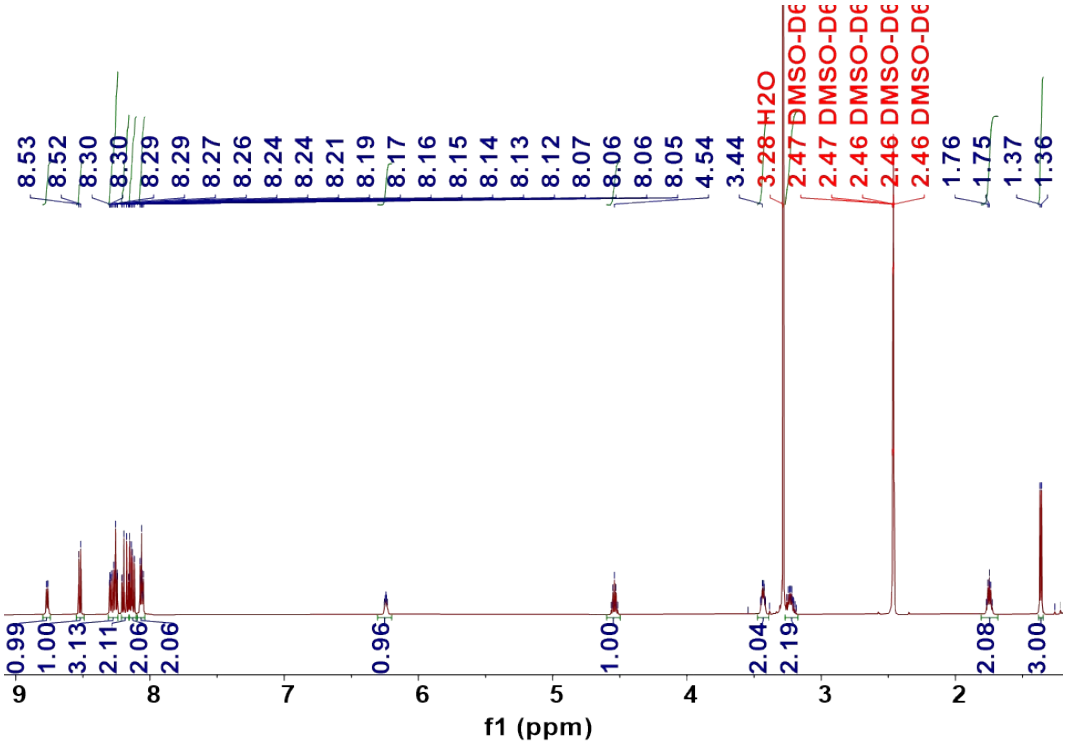

Figure S11. ^{1}H NMR of ^{L}PMA

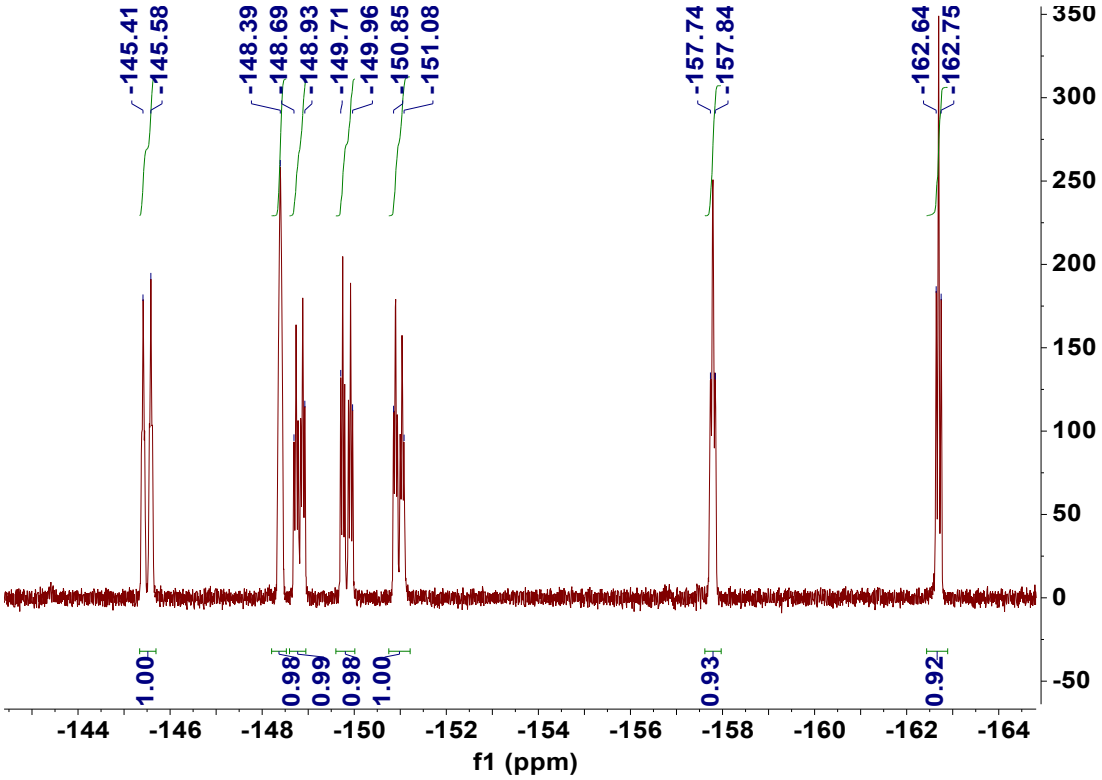

Figure S12. ^{19}F NMR of ^{L}PMA

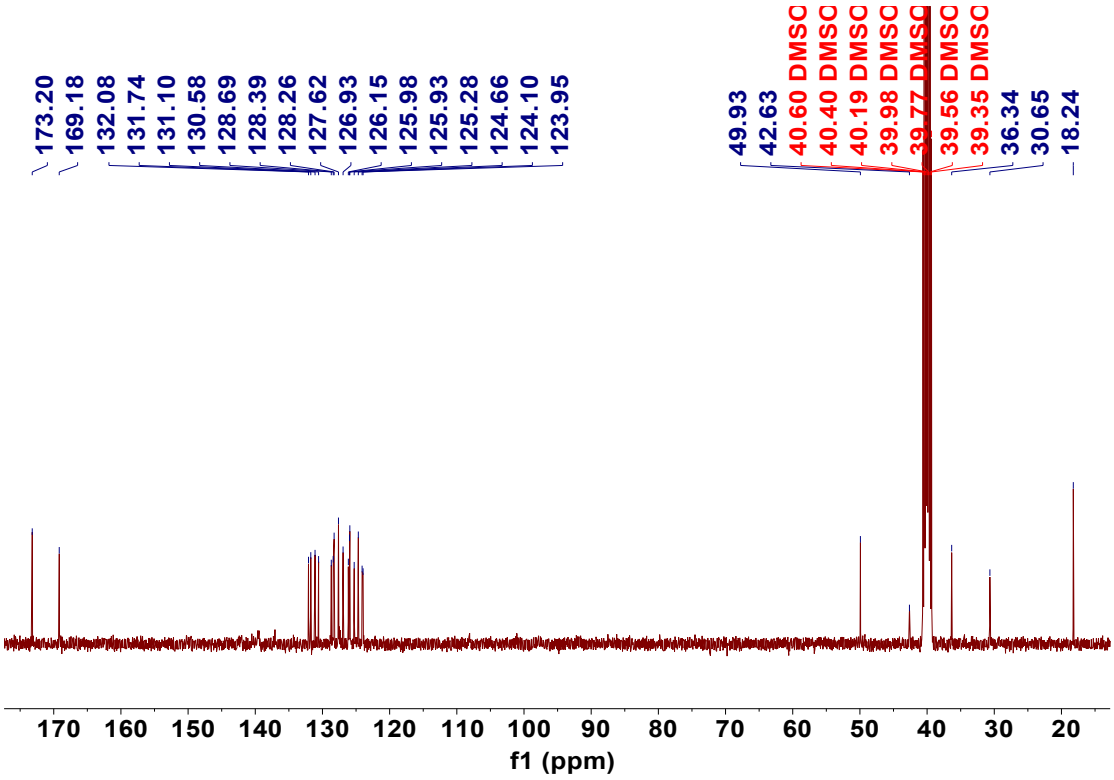

Figure S13. ^{13}C NMR of ^{L}PMA

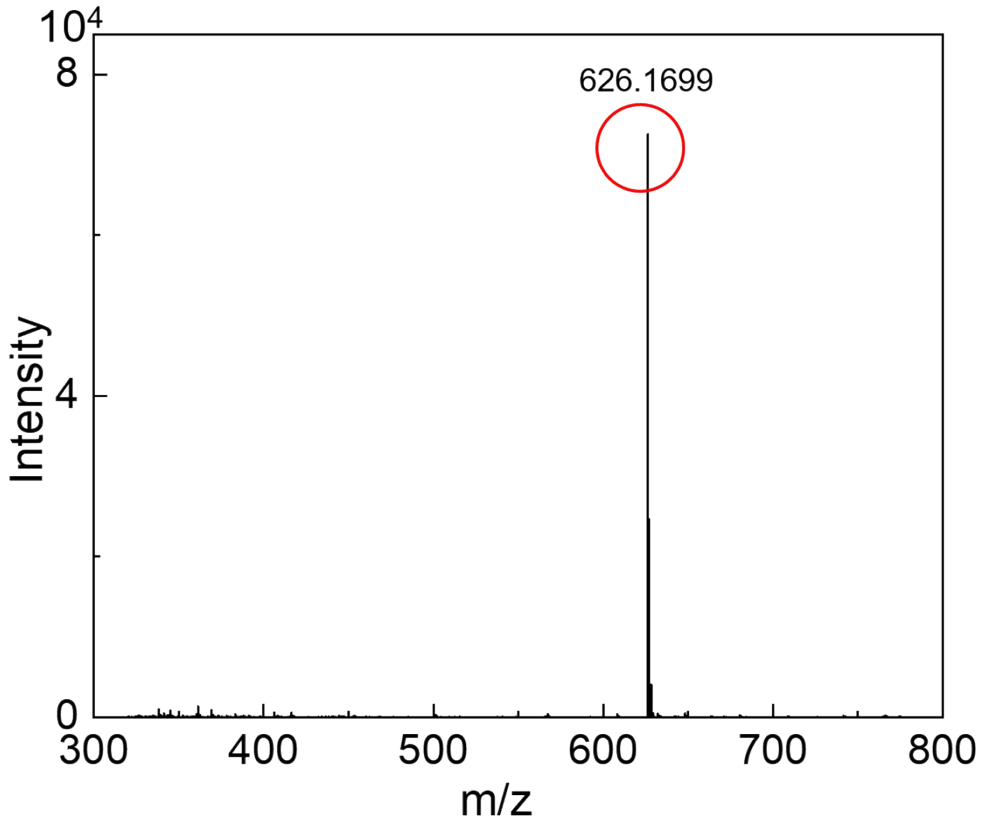

Figure S14. HRMS (TOF) of ^{L}PMA

^{L}PBA was prepared successfully with the similar method of ^{L}PMA. FN (852 mg, 2 mM) was mixed with TFA (5 mL) for ten minutes. After evaporated solvent, ^{L}BA (653 mg, 1.5 mM), HOBT (27 mg, 0.2 mM), DMAP (24 mg, 0.2 mM), EDC (400 mg, 2 mM), Et_3N (1 mL) and DCM (40 mL) were added. The mixture was stirred at room temperature for 12 h. After evaporating solvent, the crude product was subjected to column purification to obtain white powder 0.80 g. Yield: 72 %. ^{1}H NMR (400 MHz, DMSO-d_6, 298 K) δ 8.26 (d, 1H), 8.19 (m, 3H), 8.08 (t, 3H), 8.00 (t, 3H), 7.85 (d, 1H), 6.11 (s, 1H), 4.31 (m, 1H), 3.42 (m, 2H), 3.28 (m, 2H), 3.11 (m, 2H), 2.35 (m, 2H), 1.98 (m, 2H), 1.70 (m, 2H), 1.25 (d, 3H). ^{19}F NMR (376 MHz, DMSO-d_6, 298 K) δ -145.50 (d, 1F), -148.39 (s, 1F), -148.81 (m, 1F), -149.84 (m, 1F), -150.97 (m, 1F), -157.79 (t, 1F), -162.69 (t. 1F). ^{13}C NMR (101 MHz, DMSO-d_6, 298 K) δ 173.83, 172.48, 131.03, 130.59, 129.40, 128.21, 127.61, 127.52, 127.15, 126.53, 126.27, 125.03, 124.94, 124.15, 124.11, 123.82, 35.92. HRMS (TOF) m/z $[M+H]^+$, calcd for $C_{36}H_{28}F_7N_3O_2$, 667.2070; found, 668.4451.

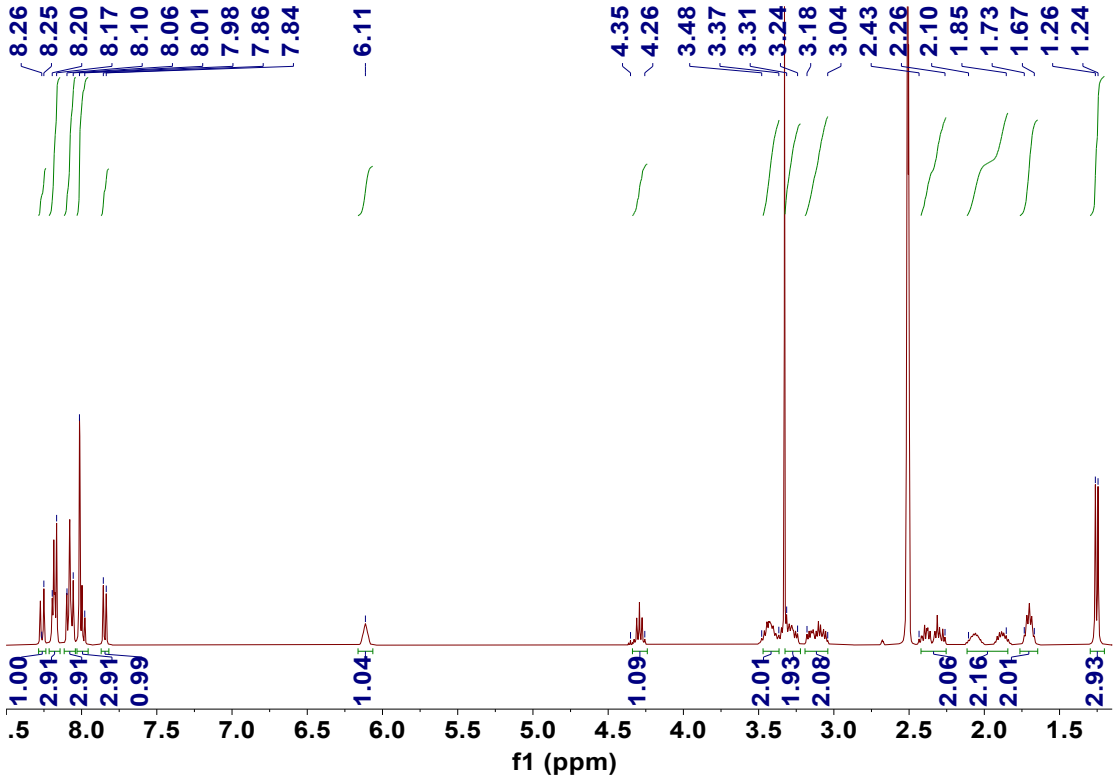

Figure S15. ^{1}H NMR of ^{L}PBA

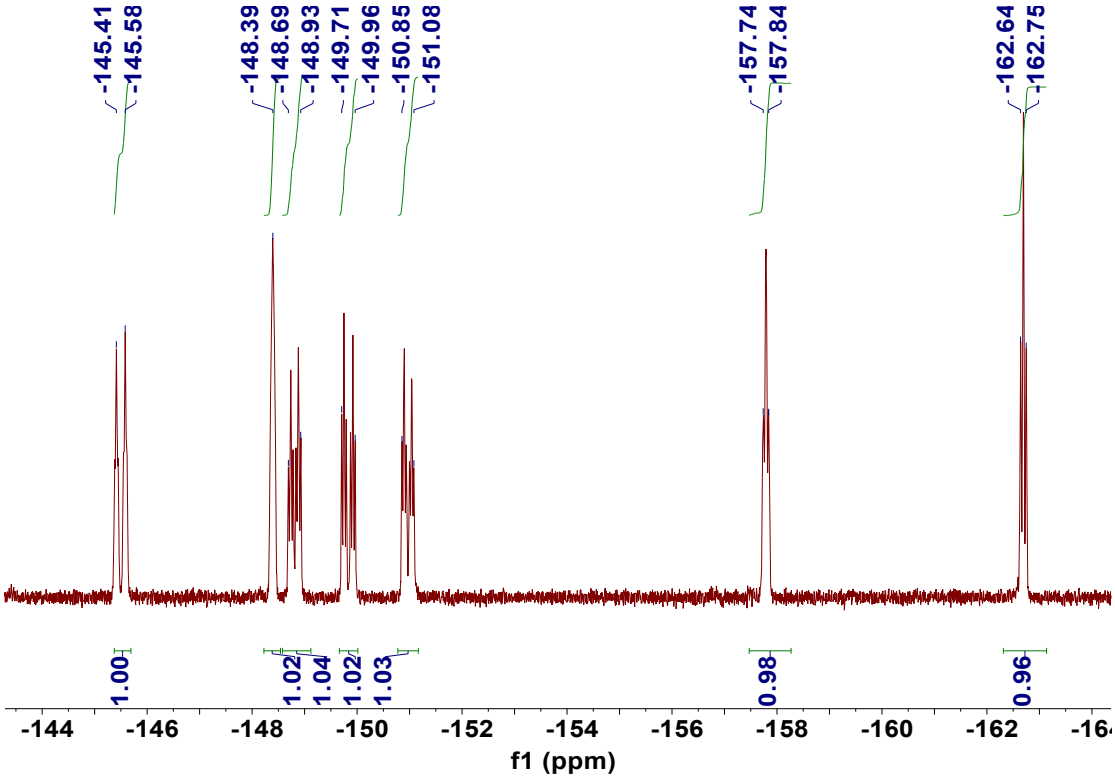

Figure S16. ^{19}F NMR of ^{L}PBA

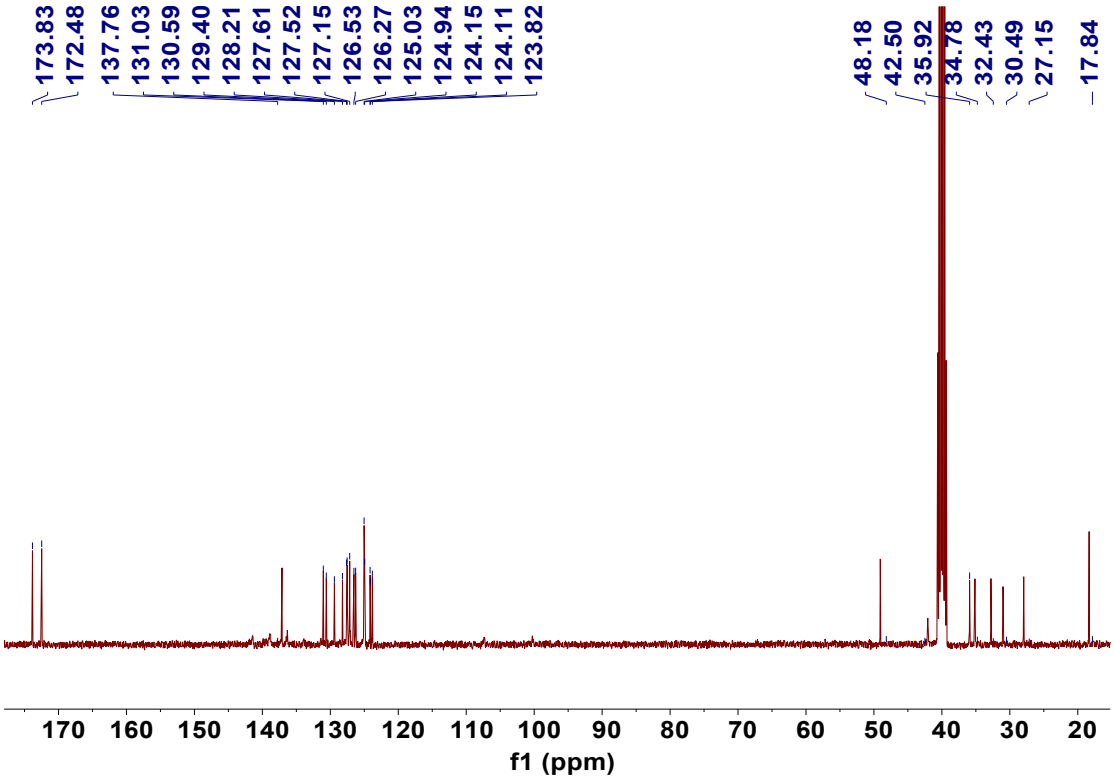

Figure S17. ^{13}C NMR of ^{L}PBA

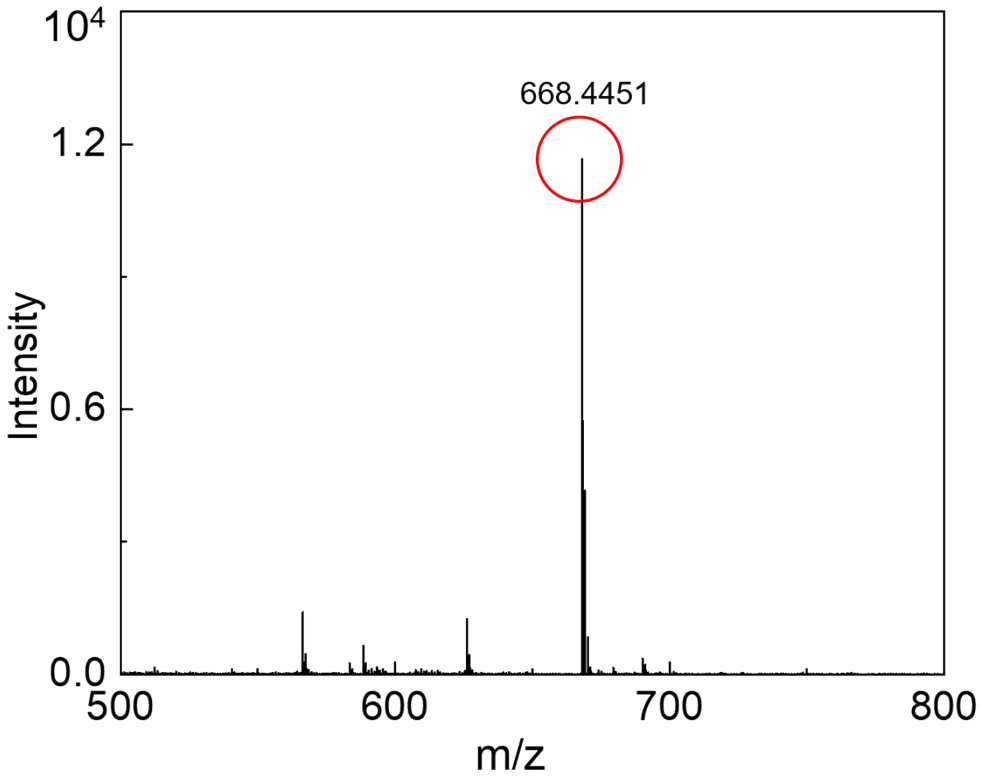

Figure S18. HRMS (TOF) of ^{L}PBA

^{D}PMA and ^{D}PBA were prepared via the same method of ^{L}PMA and ^{L}PBA,

respectively. ^{1}H NMR，^{19}F NMR and ^{13}C NMR of ^{D}PMA and ^{D}PBA were shown in Figure S13-S18.

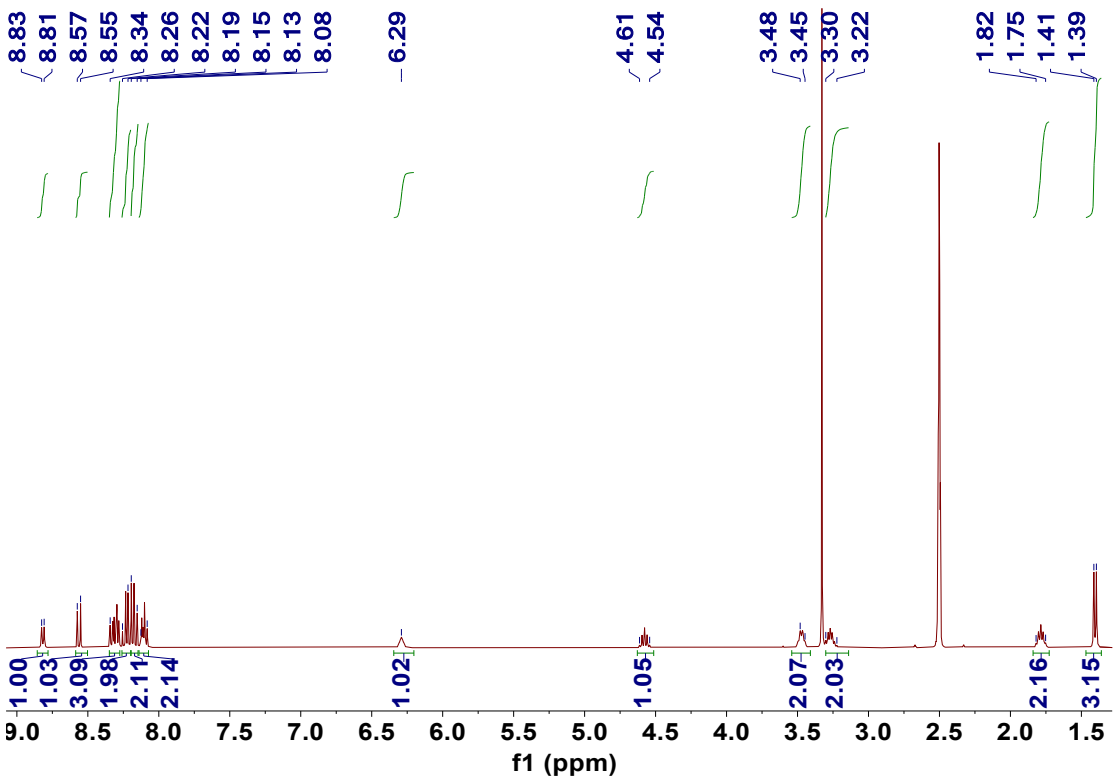

Figure S19. ^{1}H NMR of ^{D}PMA

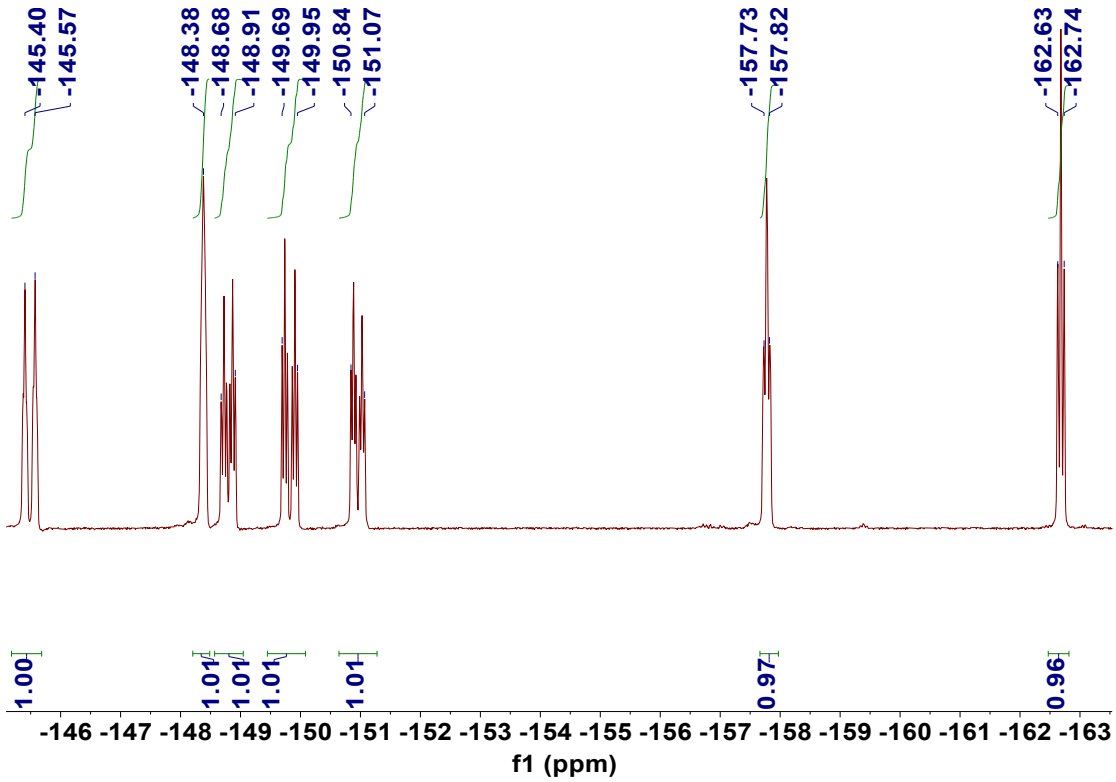

Figure S20. ^{19}F NMR of ^{D}PMA

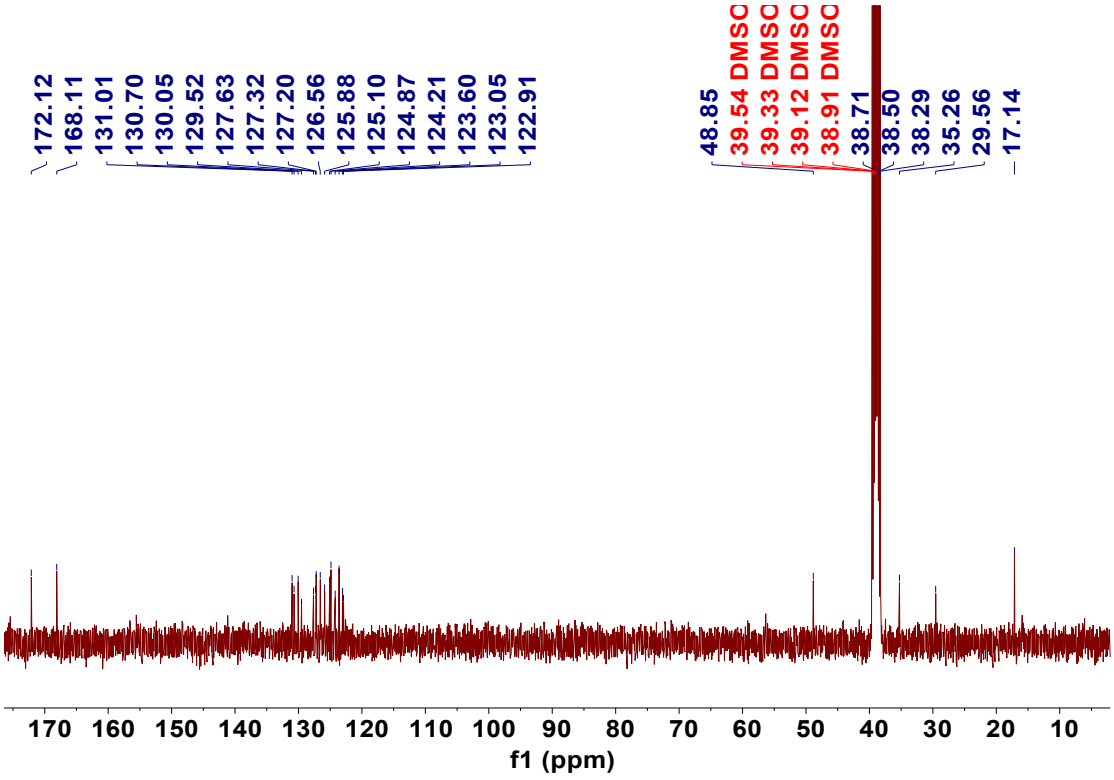

Figure S21. ^{13}C NMR of ^{D}PMA

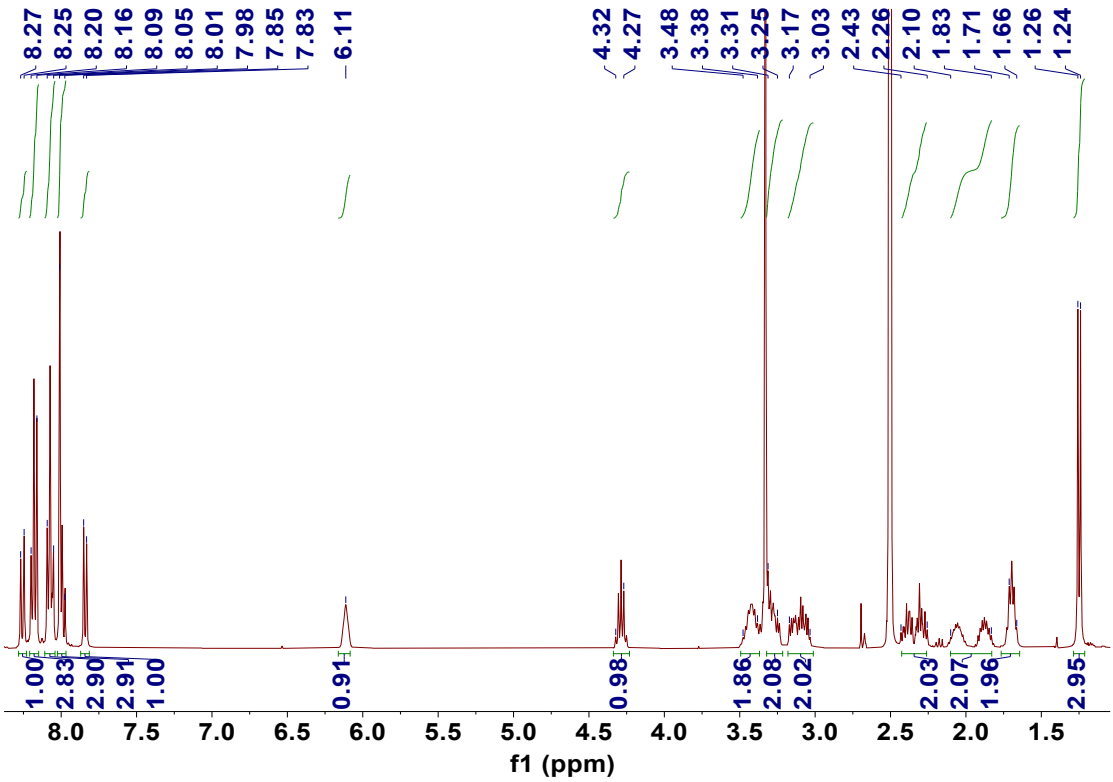

Figure S22. ^{1}H NMR of ^{D}PBA

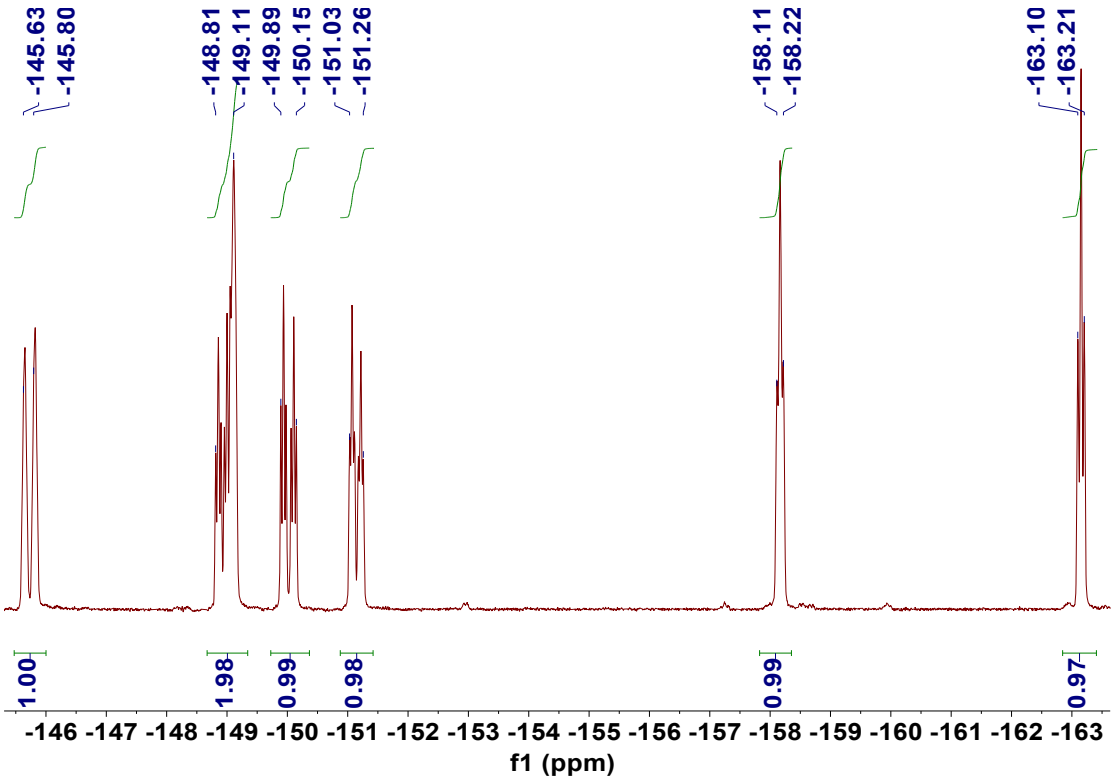

Figure S23. ^{19}F NMR of ^{D}PBA

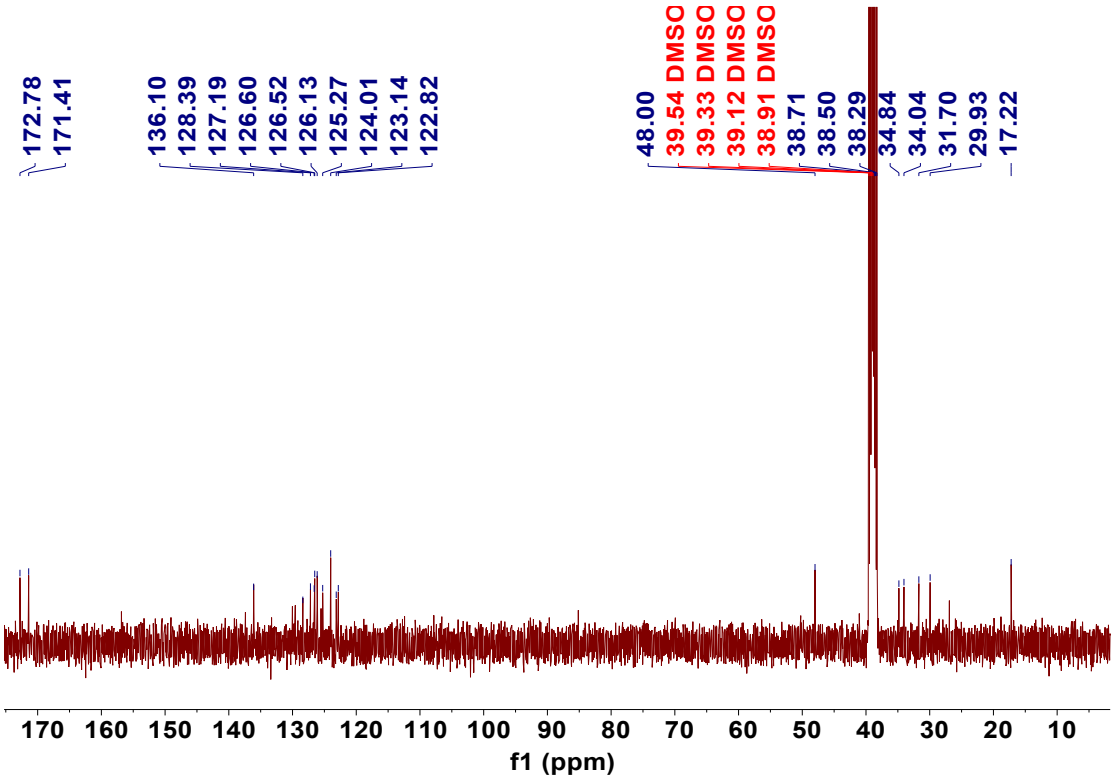

Figure S24. ^{13}C NMR of ^{D}PBA

X-ray crystallography

The single crystals of ^{L}PMA, ^{L}PBA, $^{D/L}$PMA and $^{D/L}$PBA were cultured via solvent evaporation. Single crystal with appropriate dimensions were chosen to record on a Rigaku Oxford Diffraction XtaLAB Synergy-S diffractometer at 173 K using Cu Kα (λ = 1.54184 Å) from PhotonJet micro-focus X-ray Source. The crystal data were showed in below table.

Table S1. Crystal data of ^{L}PMA

Deposition Number	2246067
Formula	C33H22F7N3O2
Temperature (K)	173
Wavelength	1.54184Å
Crystal system	triclinic
Space group	C 2 2 21
a,b,c/Å	7.1815(3) 17.3109(7) 46.2197(17)
V, Å^3	5745.95
Cell angles	90 90 90
Z, Z’	Z: 8 Z': 0
R-factor (%)	5.22

Table S2. Crystal data of $^{D/L}$PMA

Deposition Number	2246095
Formula	C33H22F7N3O2
Temperature (K)	173
Wavelength	1.54184Å
Crystal system	orthorhombic
Space group	P -1
a,b,c/Å	8.3043(2) 8.6910(2) 20.6746(4)

V, Å^3	1356.82
Cell angles	80.978(2) 81.965(2) 67.556(3)
Z, Z’	Z: 2 Z': 0
R-factor (%)	5.74

Table S3. Crystal data of ^{L}PBA

Deposition Number	2246071
Formula	2(C36H28F7N3O2)
Temperature (K)	173
Wavelength	1.54184Å
Crystal system	monoclinic
Space group	P 2_1
a,b,c/Å	17.8394(3) 8.2183(2) 22.8962(5)
V, Å^3	3272.29
Cell angles	90 102.884(2) 90
Z, Z’	Z: 2 Z': 0
R-factor (%)	11.07

Table S4. Crystal data of $^{D/L}$PBA

Deposition Number	2246072
Formula	2(C36H28F7N3O2)
Temperature (K)	173
Wavelength	1.54184Å
Crystal system	monoclinic
Space group	P 2_1
a,b,c/Å	22.8294(3) 9.44580(10) 31.1842(5)
V, Å^3	6724.53
Cell angles	90 90.301(2) 90
Z, Z’	Z: 4 Z': 0

R-factor (%)	12.82

Molecular dynamics simulation

The native structures of model compound were built from the GaussView6.0 program. The obtained configuration was optimized and the electrostatic potential (ESP) was simultaneously calculated by Hartree-Fork method. The 6-31G(d) basis set was employed in Gaussian 16 program. The Antechamber program was used to fit the restrained electrostatic potential (RESP) charge, and then the general Amber force field (GAFF) was adopted to parameterize the bonded interaction for subsequent MD simulations. The MD simulation was implemented with the GROMACS 2020 program. The long-range electrostatic interaction was calculated by the particle mesh Ewald (PME) method. The cut-off distance for non-bonded interactions was set to 1 nm. The total simulation time is 30 ns. Energy minimization was conducted using the steepest descent algorithm before performing dynamic simulation. V-rescale and Parrinello-Rahman were respectively employed to control temperature and pressure. All results were visualized using VMD program.

Theoretical calculation

Non-covalent interaction (NCI)/reduced density gradient (RDF) analysis were manipulated via Multiwfn 3.8.[1, 2] The original structures from crystal without further treatment. Input file for Multiwfn 3.8 were achieved from Gaussian 16 program[3]. Hirshfeld surfaces were calculated directly form crystals through CrystalExplorer.[4] The dimerization interaction energies were estimated via the calculation of single point energy with the B3LYP/def2svp-D3(BJ) basis set of the Gaussian 16 program. The original structures of ^{L}PMA mono, ^{L}PMA dimer and $^{D/L}$PMA dimer are directly form crystal structures.

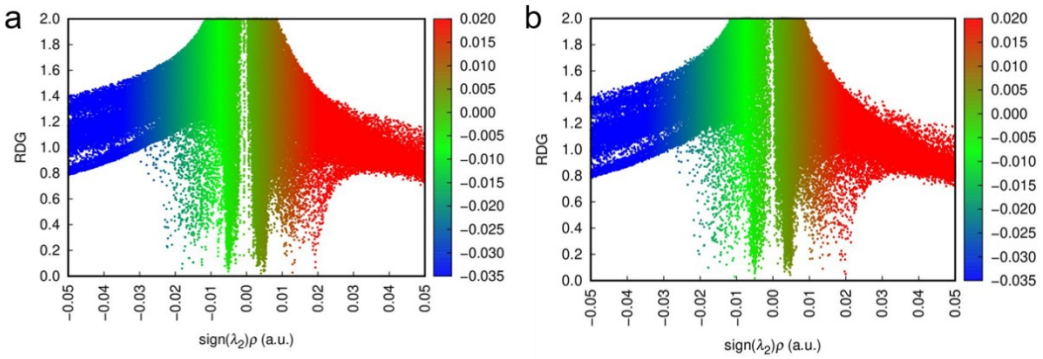

Figure S25. Scatter points images of NCI analysis including a) ^{L}PMA (dimer), b) ^{L}PBA (dimer).

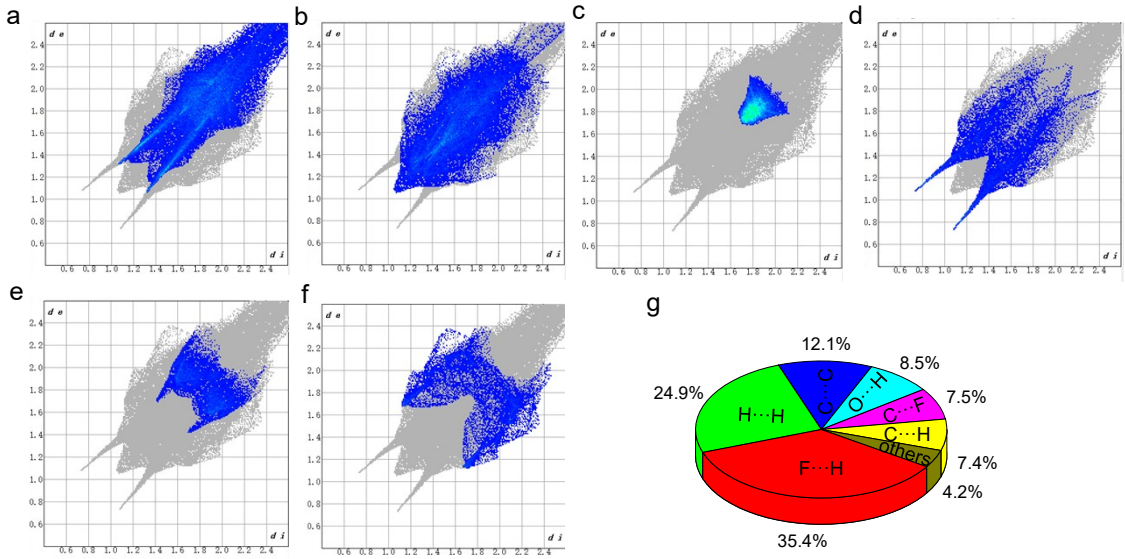

Figure S26. Surface area of reciprocal contacts from ^{L}PMA(dimer) crystal including a) F···H; b) H···H; c) C···C; d) O···H; e) C···F; f) C···H and g) the corresponding pie chart.

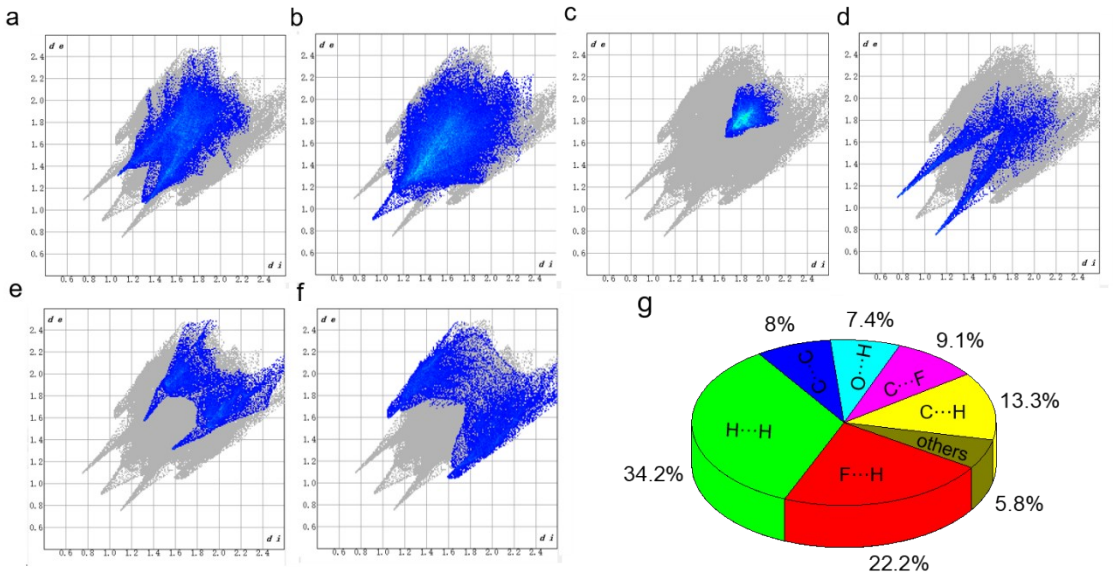

Figure S27. Surface area of reciprocal contacts from ^{L}PBA(dimer) crystal including a) F···H; b) H···H; c) C···C; d) O···H; e) C···F; f) C···H and g) the corresponding pie chart.

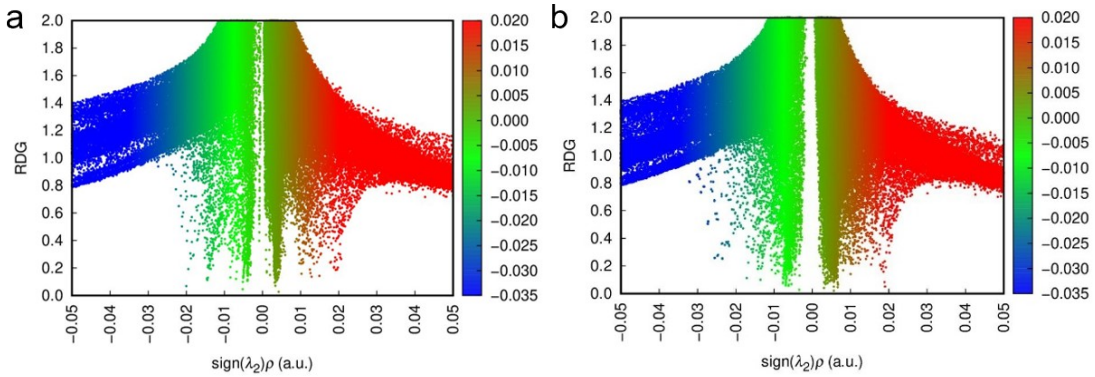

Figure S28. Scatter points images of NCI analysis including $^{D/L}$PMA(dimer), ^{L}PBA(folder) from $^{D/L}$PBA crystal.

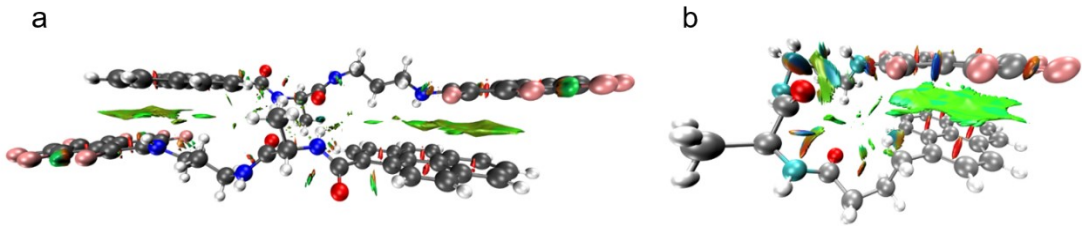

Figure S29. Noncovalent interaction analysis of $^{D/L}$PMA dimer and ^{L}PBA folder.

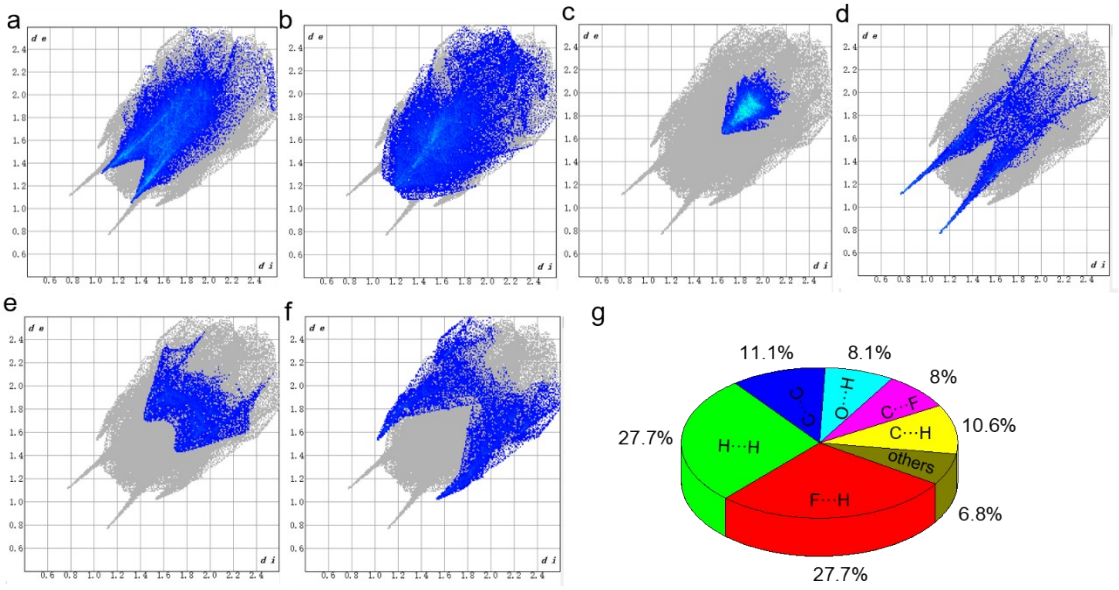

Figure S30. Surface area of reciprocal contacts from $^{D/L}$PMA(dimer) crystal including a) F···H; b) H···H; c) C···C; d) O···H; e) C···F; f) C···H and g) the corresponding pie chart.

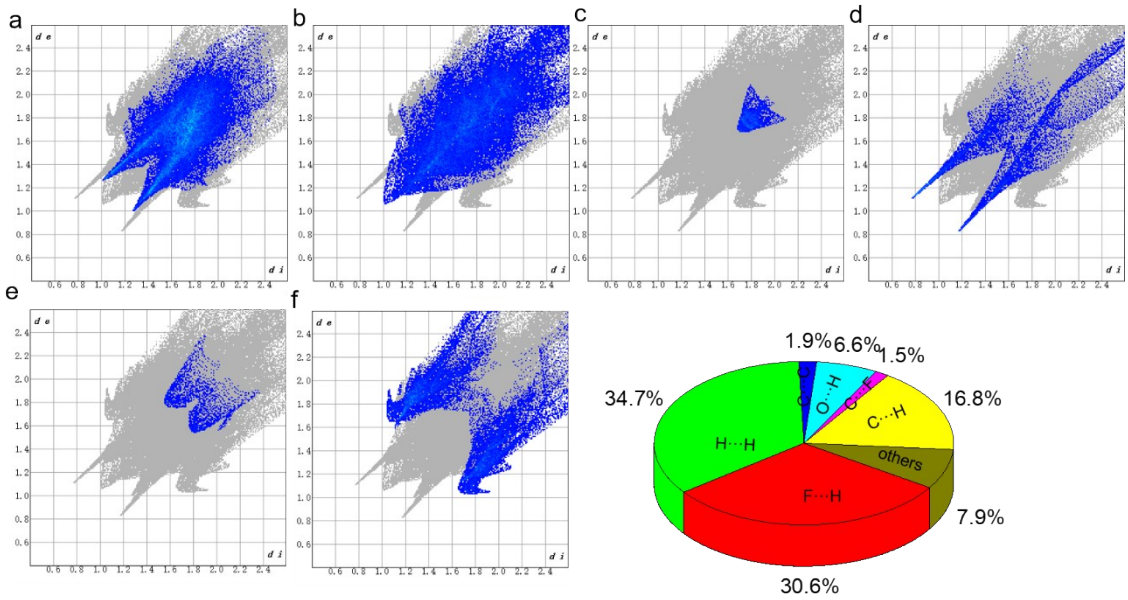

Figure S31. Surface area of reciprocal contacts of ^{L}PBA folder from $^{D/L}$PBA crystal including a) F···H; b) H···H; c) C···C; d) O···H; e) C···F; f) C···H and g) the corresponding pie chart.

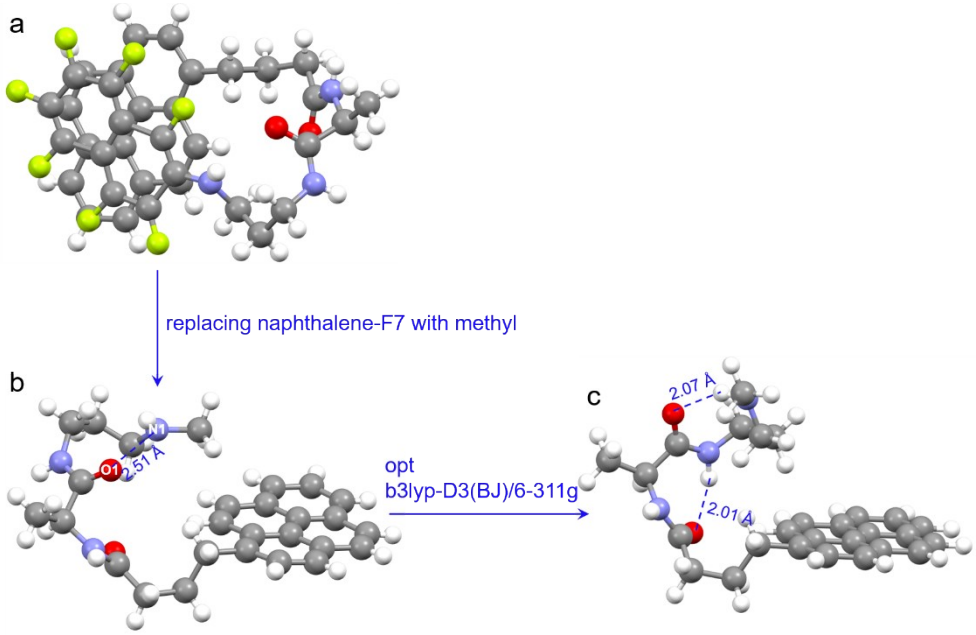

Figure S32. a) ^{L}PBA folded structure from $^{D/L}$PBA crystal; b) Simulated model after replacing naphthalene-F7 with methyl; c) Optimizing the structure with b3lyp-D3(BJ)/6-311g.

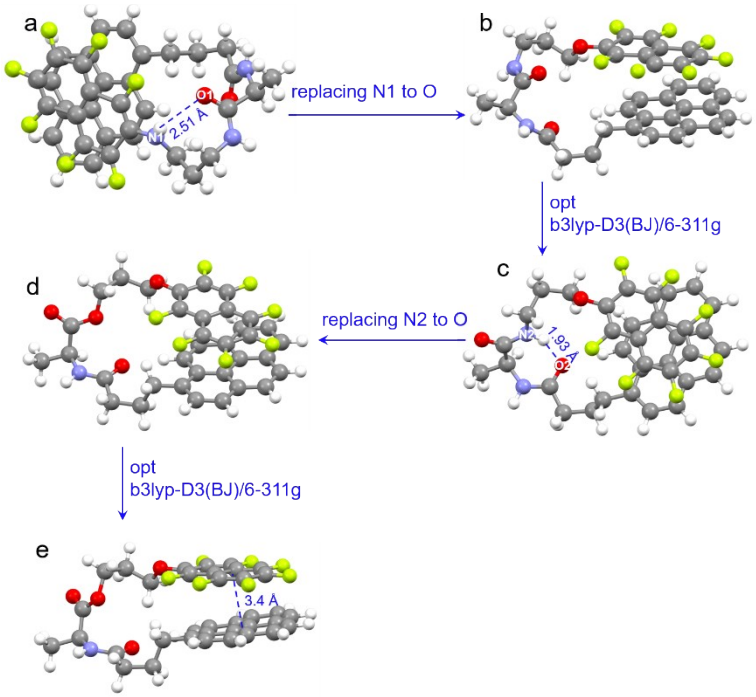

Figure S33. a) ^{L}PBA folded structure from $^{D/L}$PBA crystal; b) Simulating model and c) optimizing structure with b3lyp-D3(BJ)/6-311g after replacing N1 to O; d) Simulating model and e) optimizing structure with b3lyp-D3(BJ)/6-311g after replacing N2 to O.

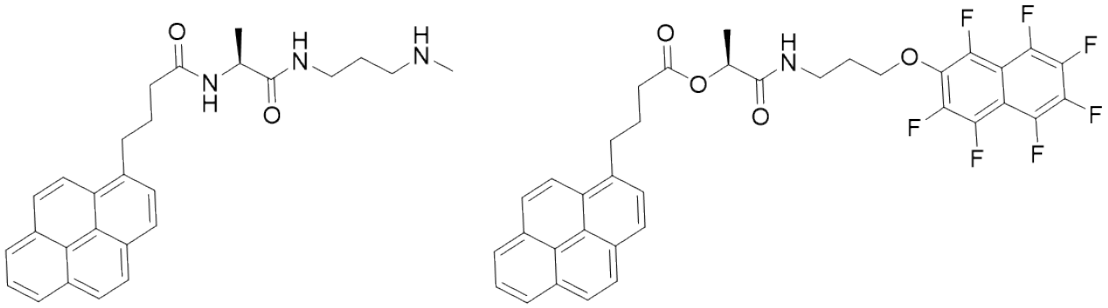

Figure S34. The chemical structure of model compounds.

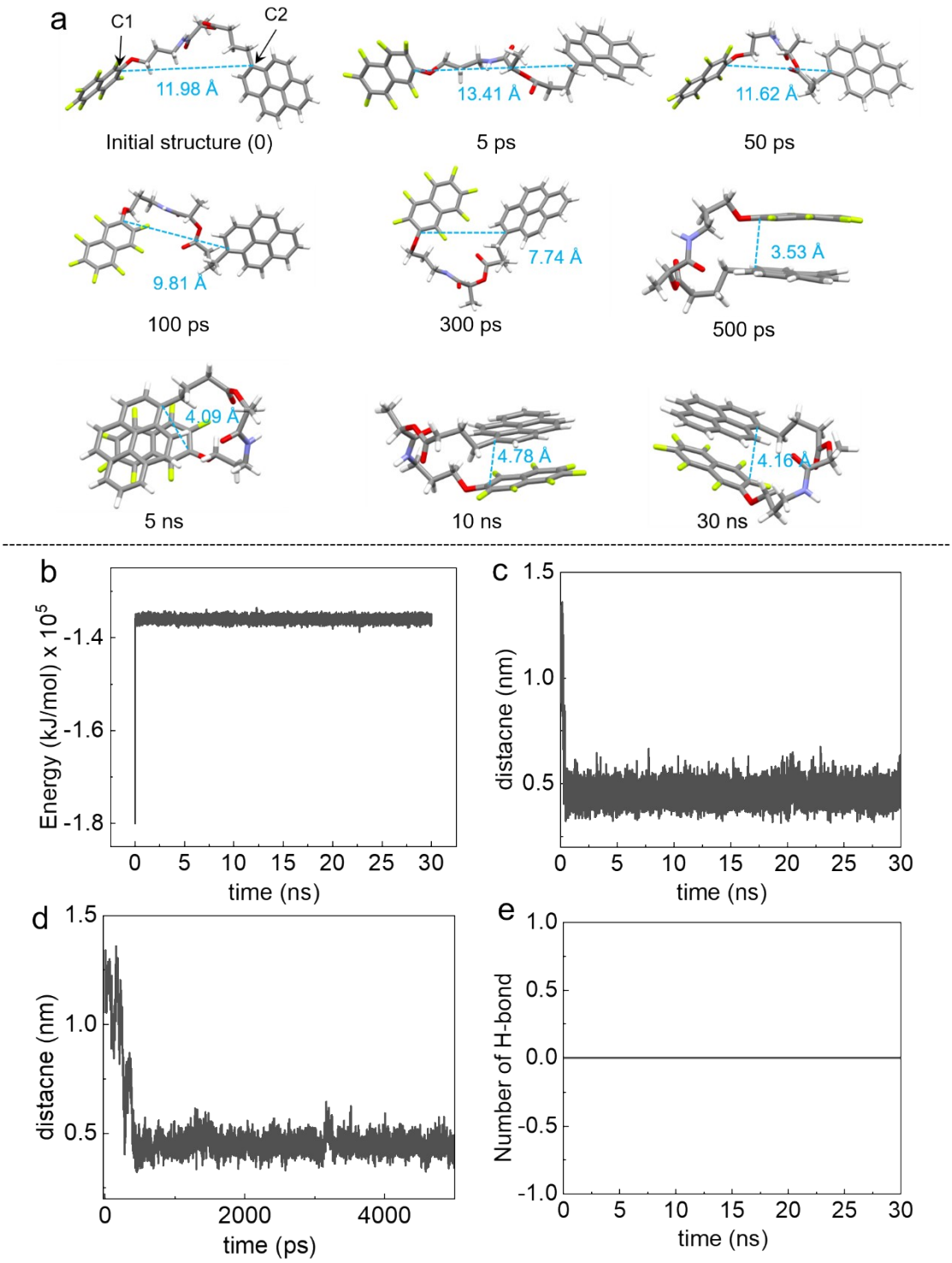

Figure S35. Molecular dynamic simulation. (a) Structure evolution process with time. Variation of (b) energy (c, d). Distance between C1 and C2 and (e) number of H-bond for simulation system.

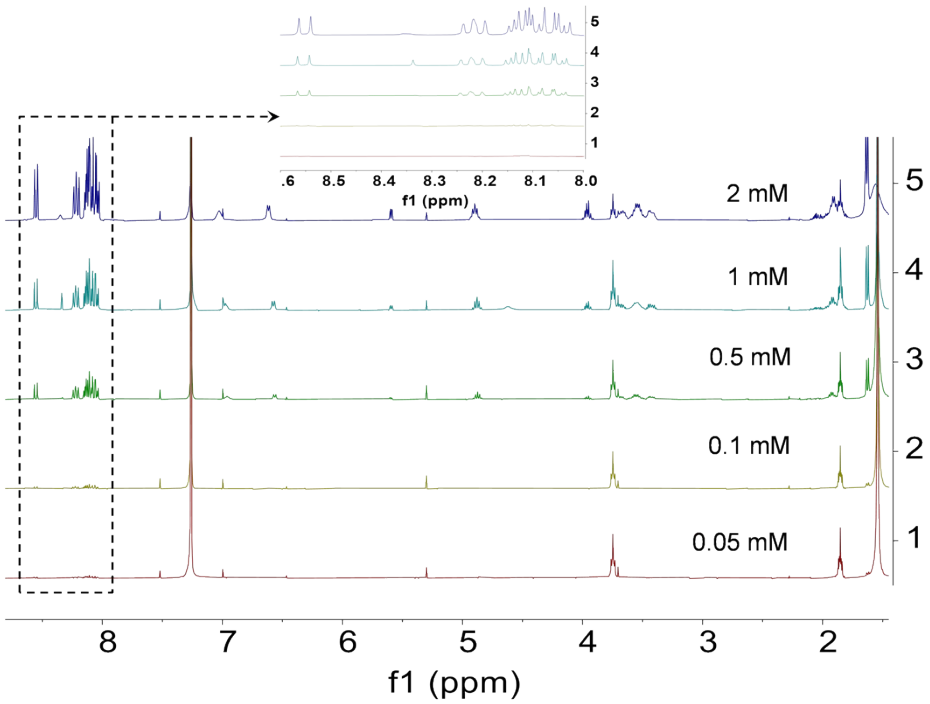

Figure S36. Concentration dependent ^{1}H NMR spectra of ^{L}PMA form 0.05 mM to 2.0 mM in $CDCl_3$

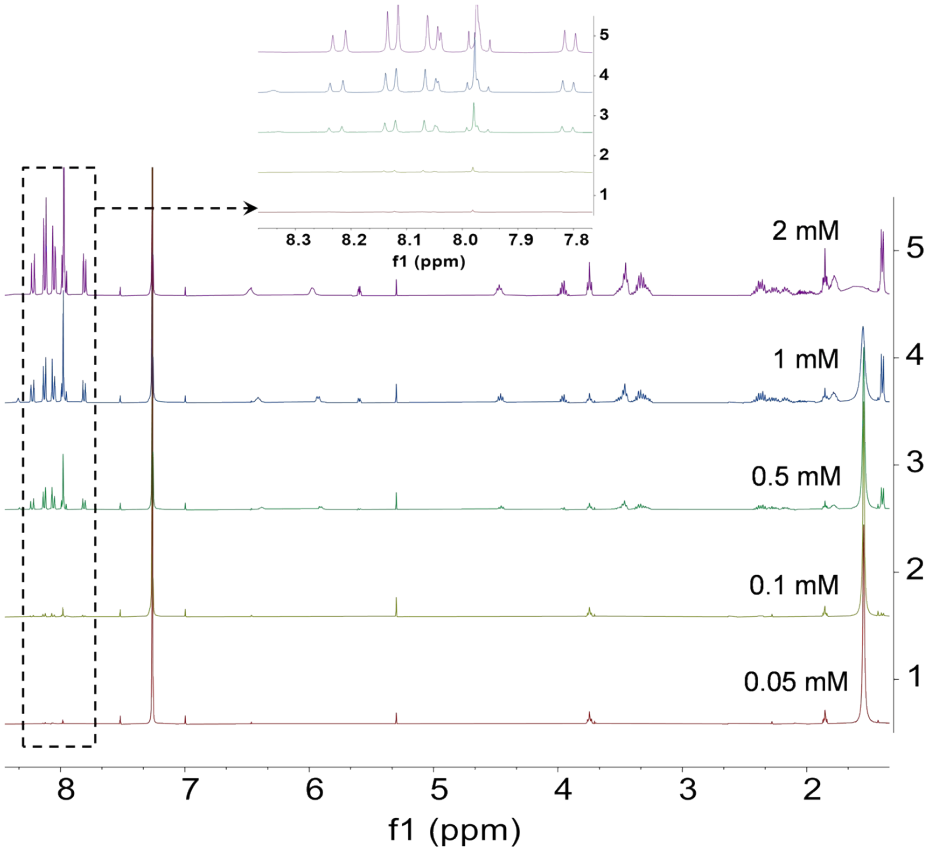

Figure S37. Concentration dependent ^{1}H NMR spectra of ^{L}PBA form 0.05 mM to 2.0 mM in $CDCl_3$

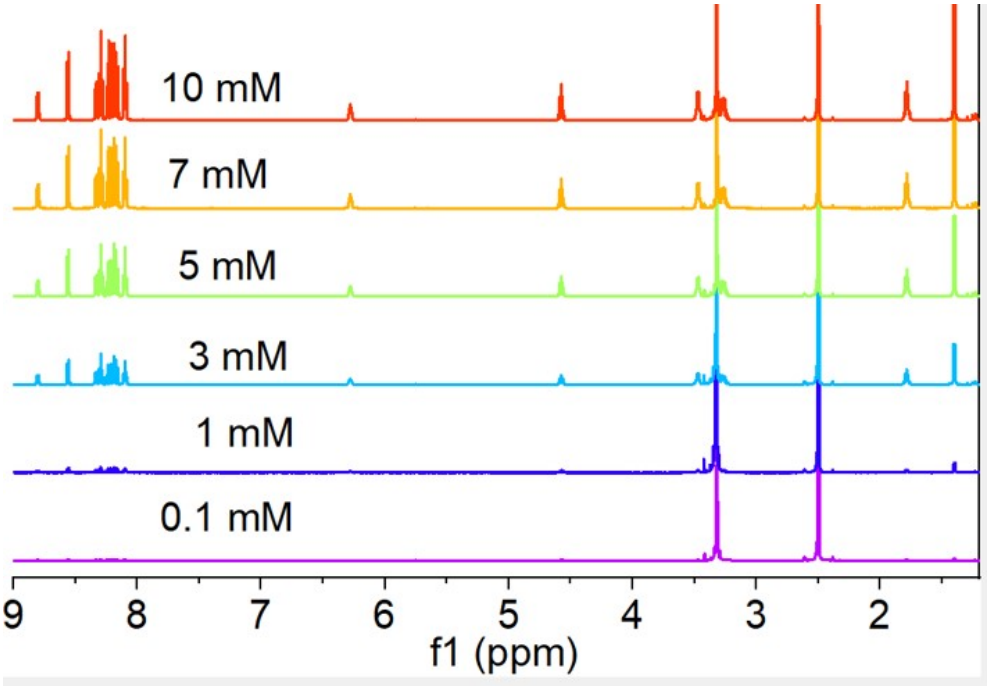

Figure S38. Concentration dependent ^{1}H NMR spectra of ^{L}PMA including 0.1 mM, 1 mM, 3 mM, 5 mM, 7 mM and 10 mM in DMSO-d_6.

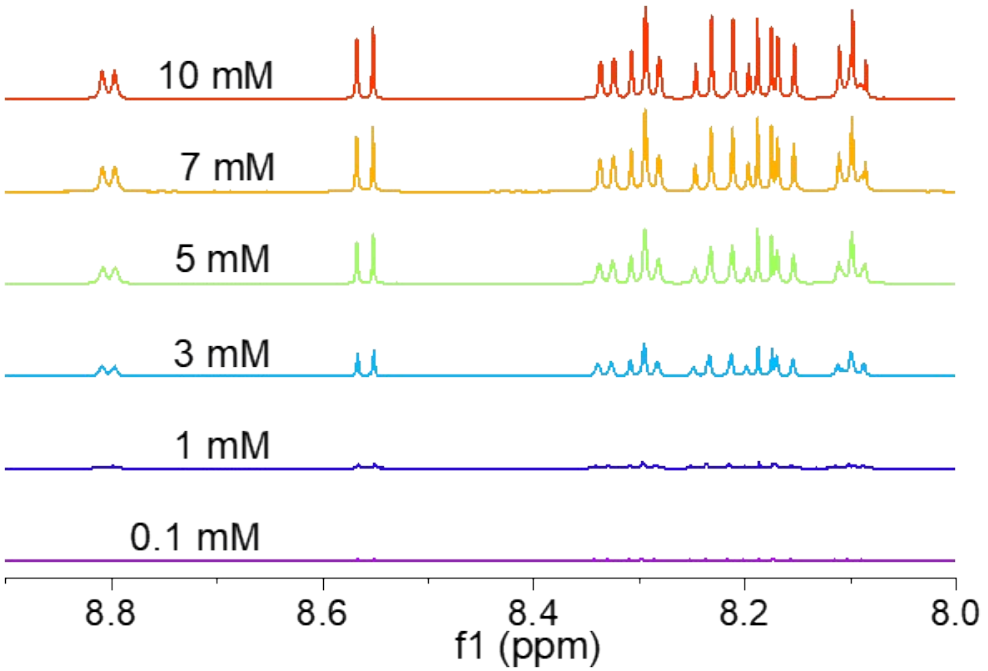

Figure S39. Concentration dependent ^{1}H NMR spectra of ^{L}PMA including 0.1 mM, 1 mM, 3 mM, 5 mM, 7 mM and 10 mM in DMSO-d_6.

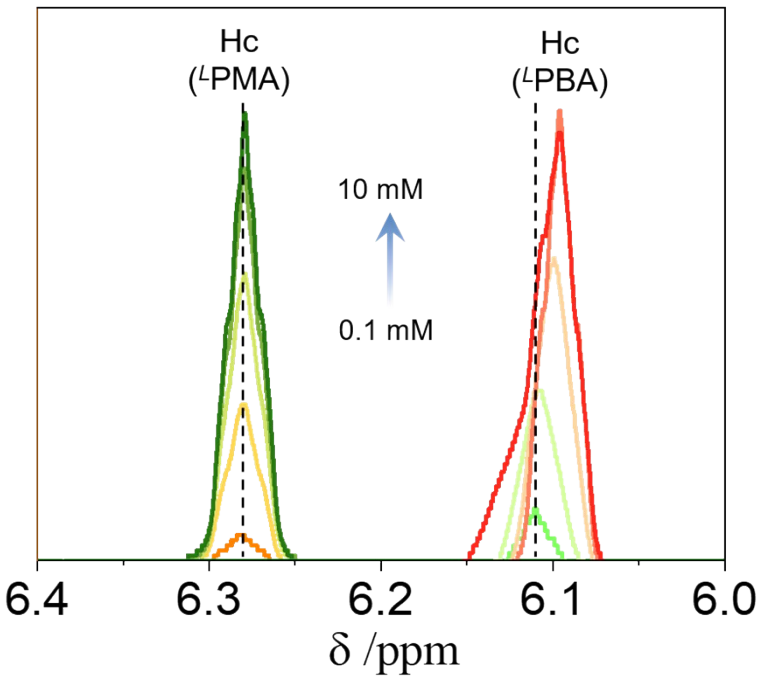

Figure S40. Partial concentration-dependent ^{1}H NMR spectra of ^{L}PMA and ^{L}PBA in DMSO-d_6

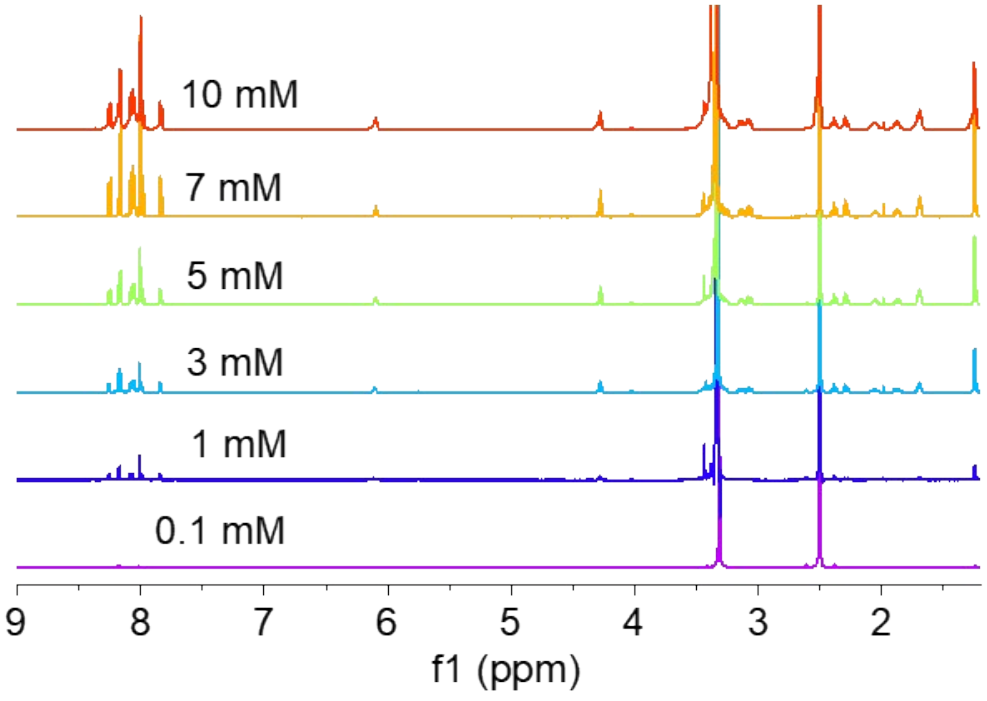

Figure S41. Concentration dependent ^{1}H NMR spectra of ^{L}PBA including 0.1 mM, 1 mM, 3 mM, 5 mM, 7 mM and 10 mM in DMSO-d_6.

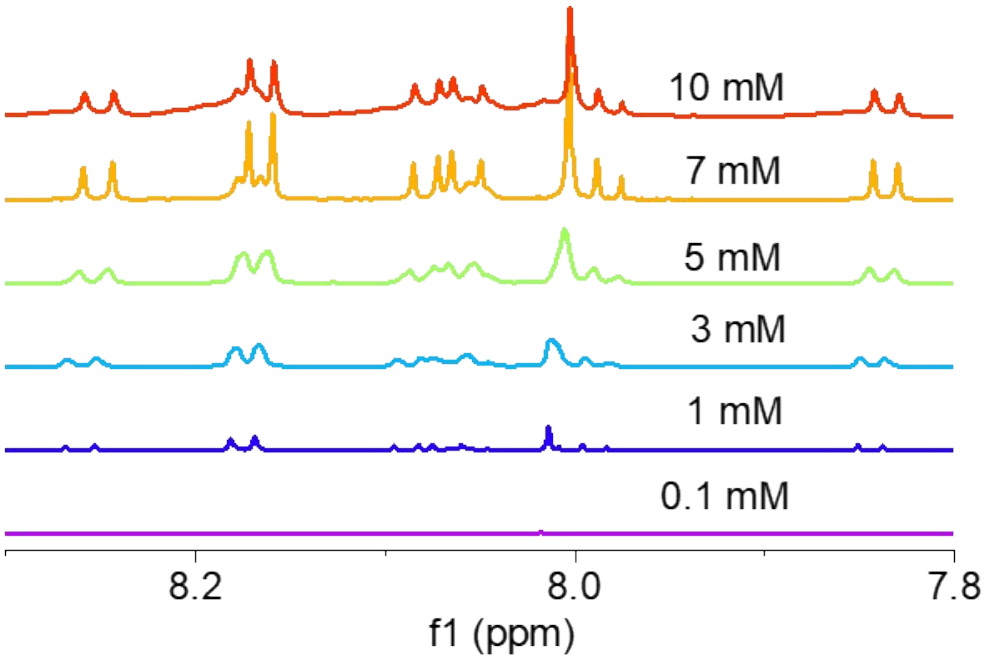

Figure S42. Concentration dependent ^{1}H NMR spectra of ^{L}PBA including 0.1 mM, 1 mM, 3 mM, 5 mM, 7 mM and 10 mM in DMSO-d_6.

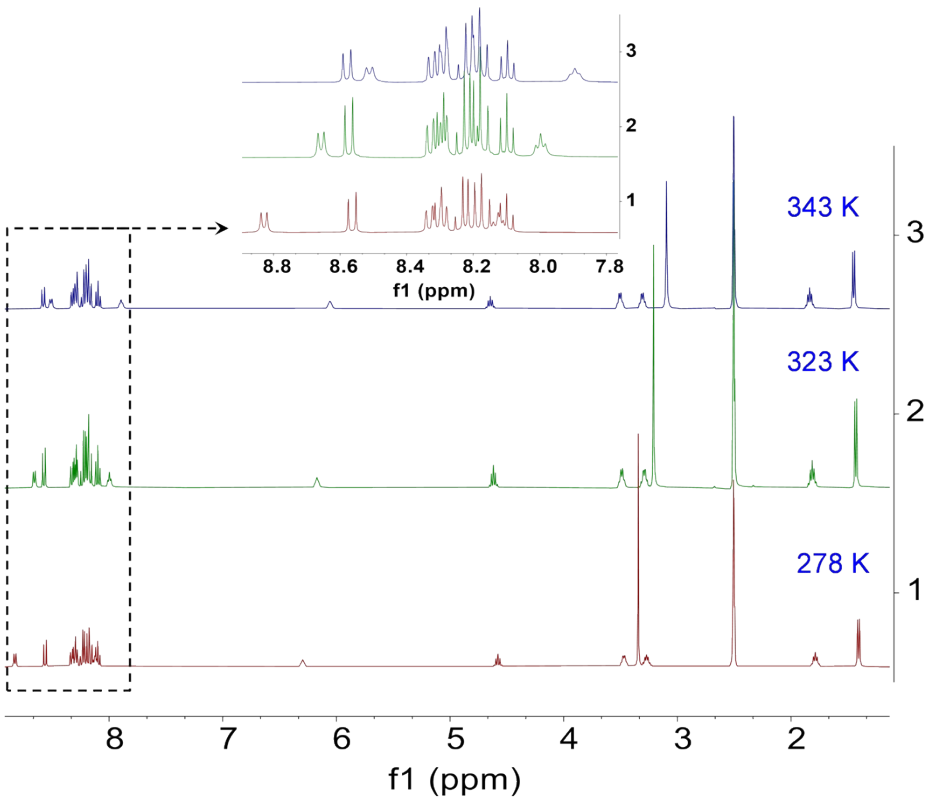

Figure S43. Temperature-variable ^{1}H NMR spectra of ^{L}PMA in DMSO-d_6 (10 mM)

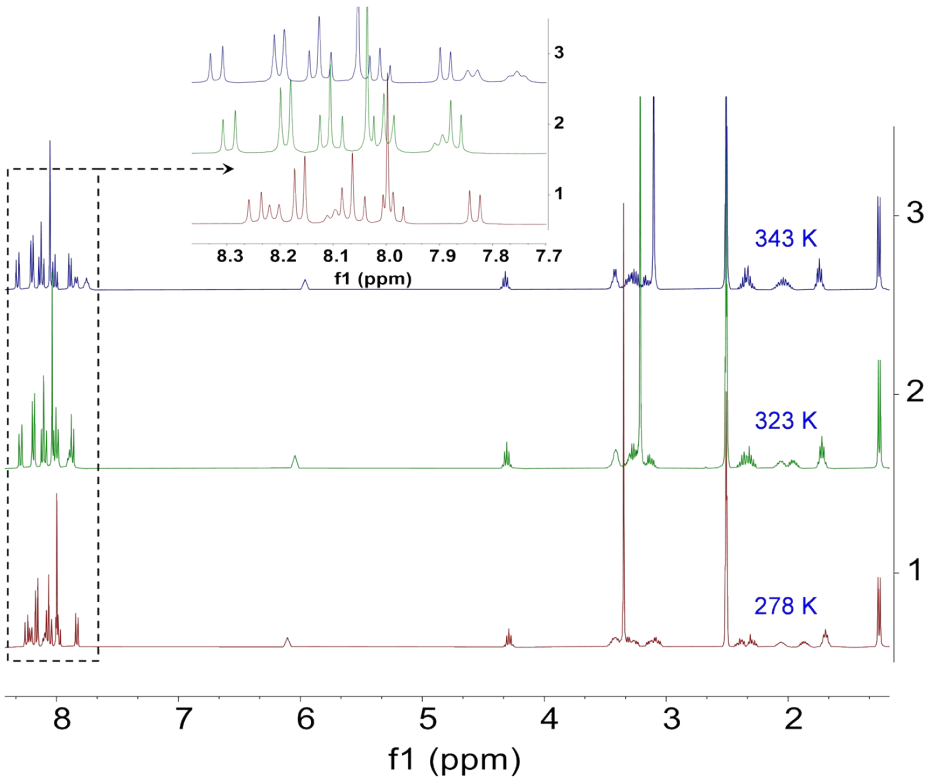

Figure S44. Temperature-variable ^{1}H NMR spectra of ^{L}PBA in DMSO-d_6 (10 mM).

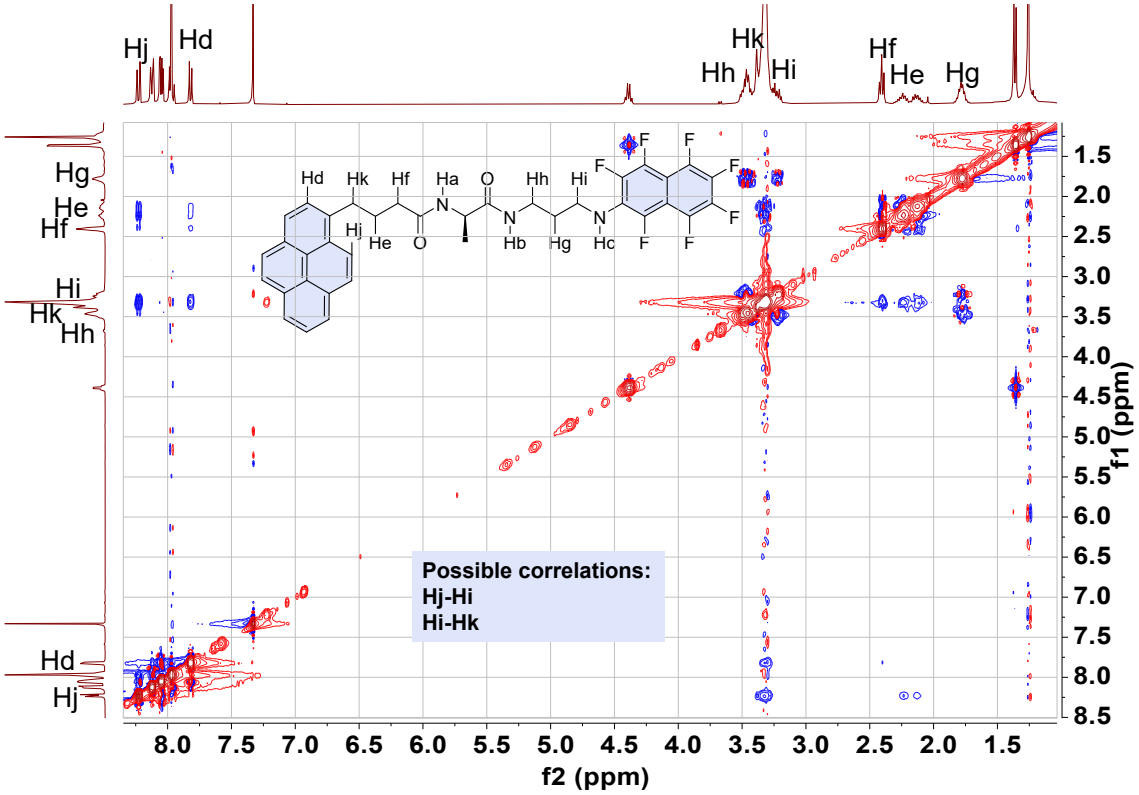

Figure S45. 2D NOESY spectra of ^{L}PBA in $CDCl_3/CH_3OD$ (9/1, 10 mM).

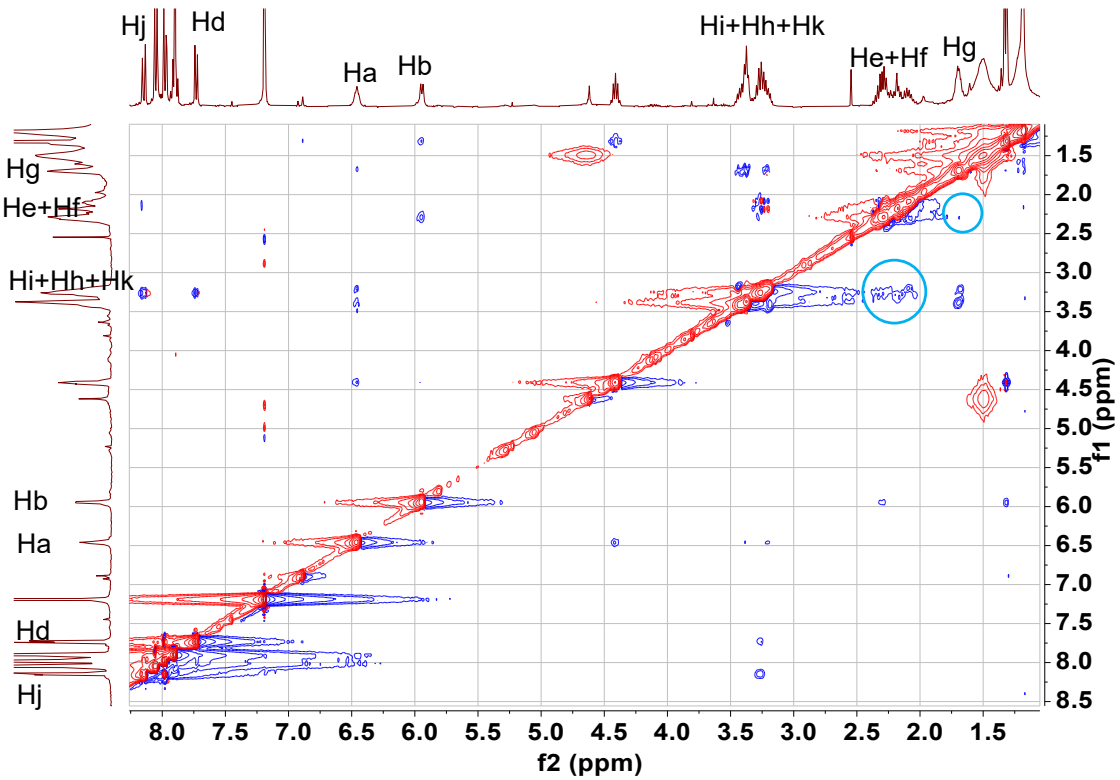

Figure S46. 2D NOESY spectra of ^{L}PBA in $CDCl_3$ (saturated) (cyan regions are possible corrections to prove existing of dimer).

Fitting procedures to derive size parameters form log D[5-7]

Stocks-Einstein equation build a relationship between diffusion coefficient and hydrodynamic radius with sphere model:

$$D = \frac{k_b T}{6\pi\eta r_h(sp)}$$

Where k_B is the *Boltzmann* constant (k_B = 1.38 × 10^{-23}), , T is temperature (K), η is viscosity of the solvent, and $r_h(sp)$ is the hydrodynamic radius.

The equation can be modified for oblate spheroid model:

$$D = \frac{k_b T}{c f_s \pi\eta r_h(ob)}$$

Where

$$c = \frac{6}{1 + 0.695\left(\frac{r_{vdW}}{r_h(ob)}\right)^{2.234}}$$

$c \approx 6$, because r_{vdW} (van der Waals radius of the solvent) is far less than the

hydrodynamic radius of the molecules which are investigated. Thus:

$$r_h(ob) = \frac{r_h(sp)}{f_s}$$

$$f_s = \frac{\sqrt{(\frac{b}{a})^2 - 1}}{(\frac{b}{a})^{\frac{2}{3}} \tan^{-1}\sqrt{(\frac{b}{a})^2 - 1}}$$

a and b are the semiminor and semimajor axis of the oblate spheroid.

The following figures shows the result for hydrodynamic radii of PMA and PBA in DMSO and $CHCl_3$ with various temperature. Viscosity information get from fitting curves of DMSO and $CHCl_3$ upon various temperature. *r*(cal) is the radius of a sphere with an equivalent volume as the spheroid generated by a and b; spheroid volume ($V = \frac{4}{3}\pi ab^2$); $r(cal) = \sqrt[3]{\frac{3V}{4\pi}} = \sqrt[3]{ab^2}$. Ratio of the hydrodynamic radius generated from the oblate model (*r*h(ob)) and the equivalent radius generated by the volume of the spheroid (*r*(cal)) was used to guide the adjustment of a and b until the volume generated by them matches the volume generated by *r*h(ob) (*r*h(ob)/*r*(cal) ≈ 1)

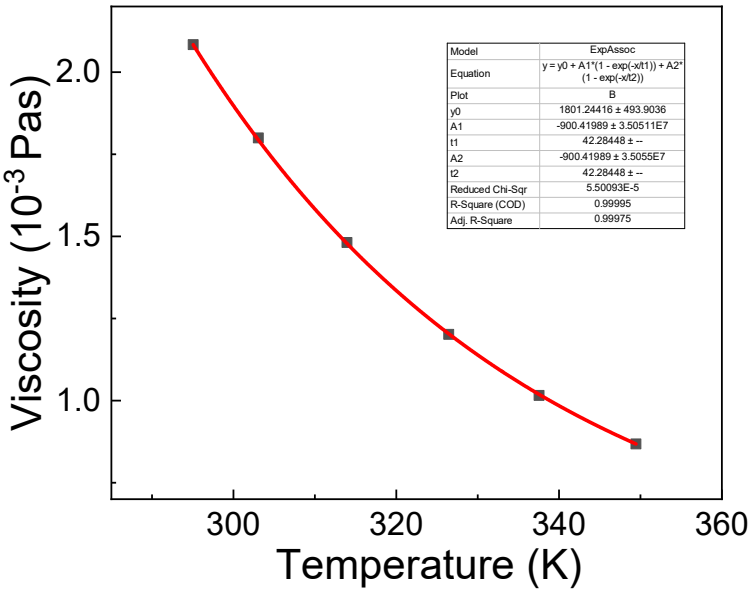

Figure S47. Fitting of viscosity versue temperature data for DMSO based on values found in the literature[8].

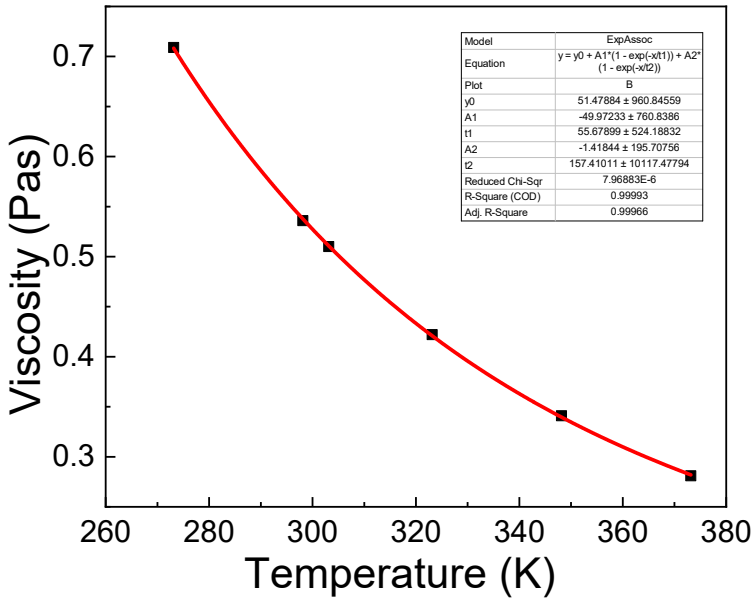

Figure S48. Fitting of viscosity versue temperature data for $CHCl_3$ based on values found in the literature[9].

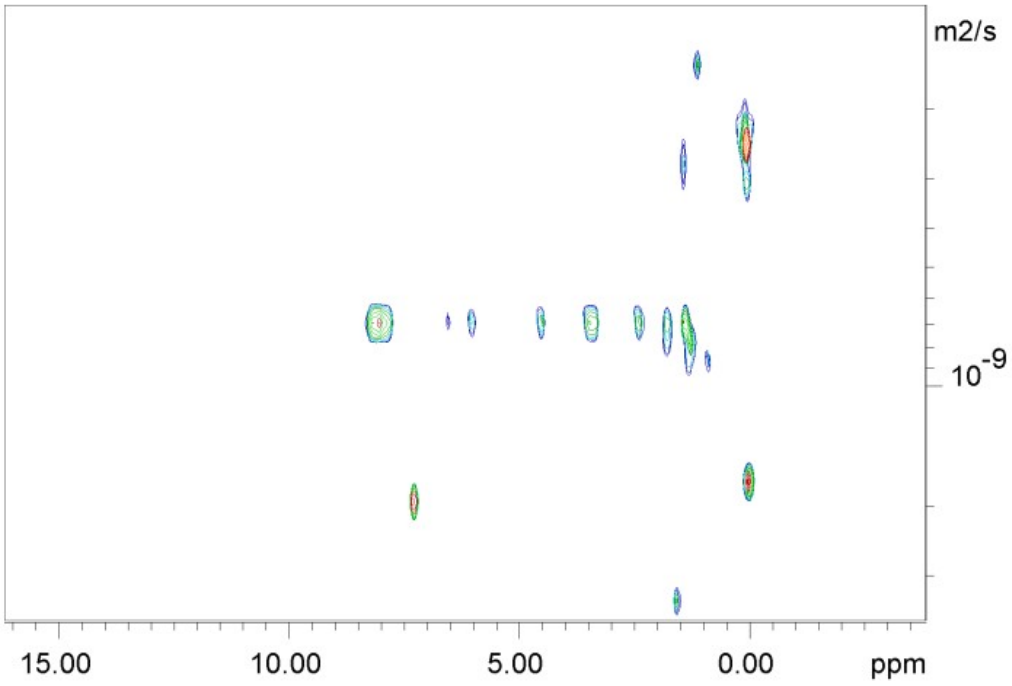

Figure S49. DOSY NMR spectra of ^{L}PMA in $CDCl_3$ with 298.15 K.

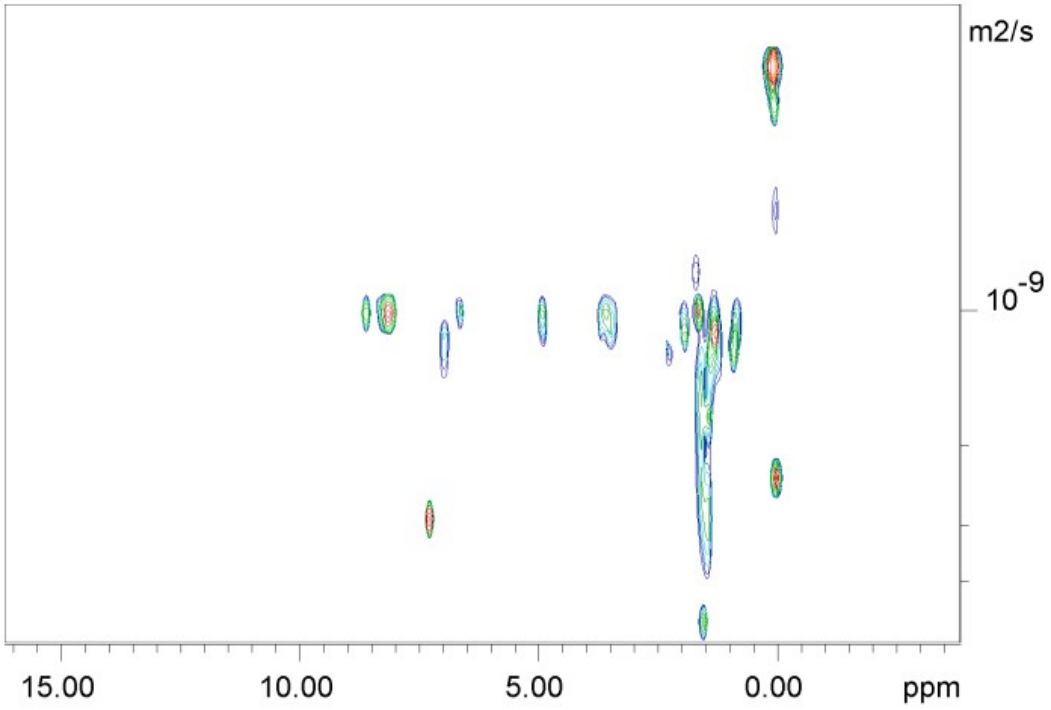

Figure S50. DOSY NMR spectra of ^{L}PMA in $CDCl_3$ with 318.15 K.

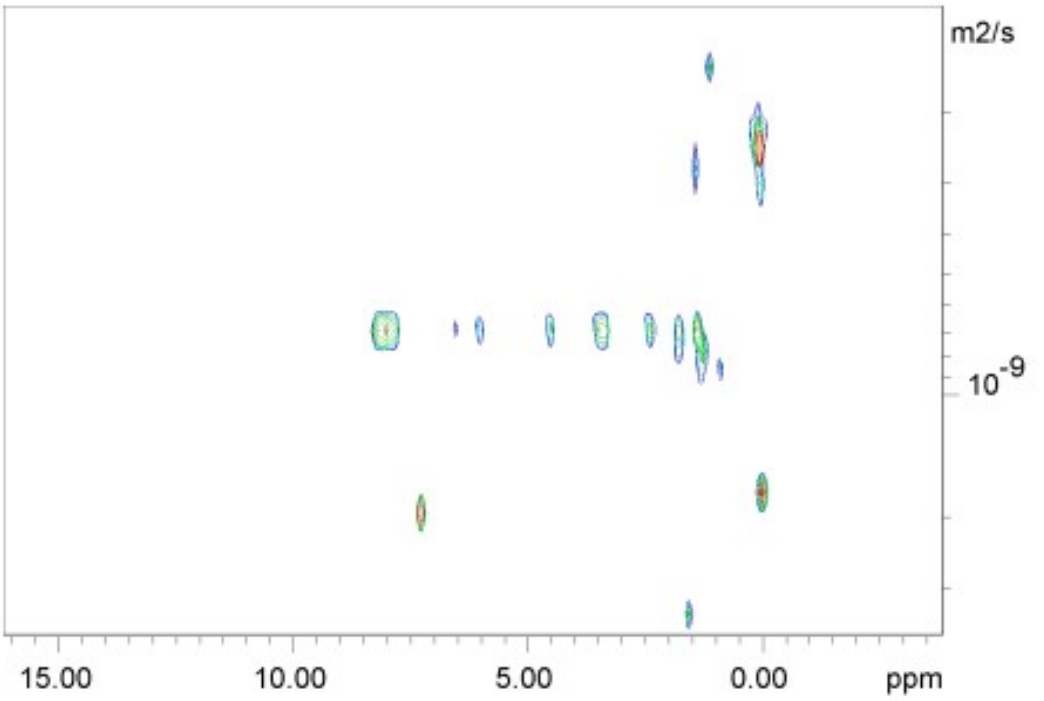

Figure S51. DOSY NMR spectra of ^{L}PBA in $CDCl_3$ with 298.15 K.

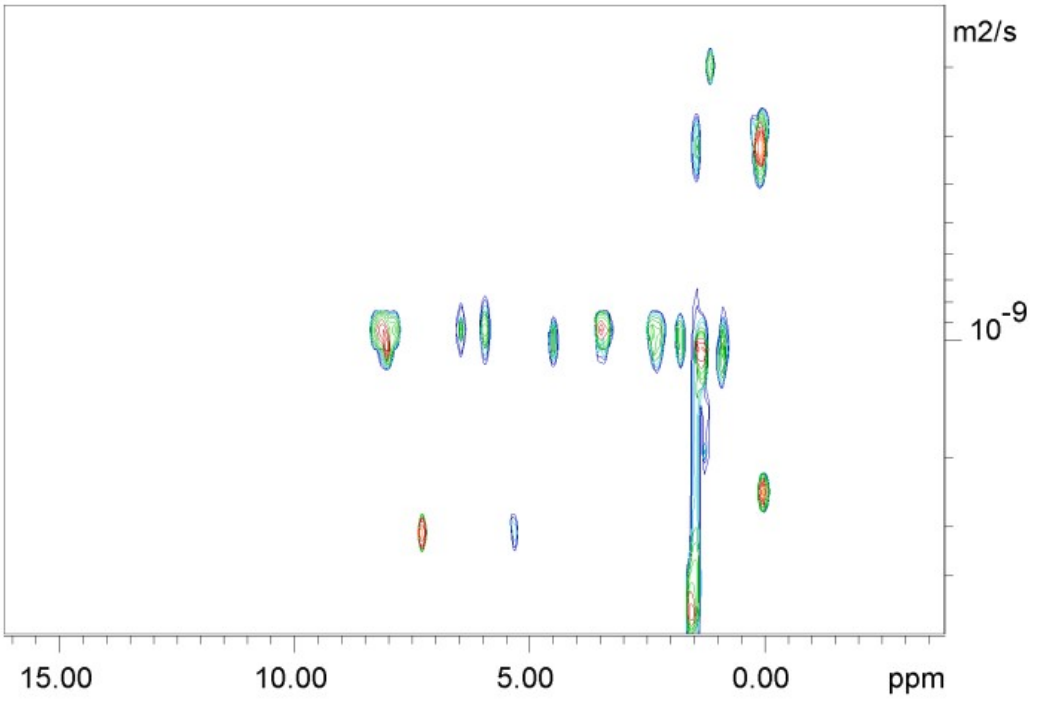

Figure S52. DOSY NMR spectra of ^{L}PBA in $CDCl_3$ with 318.15 K.

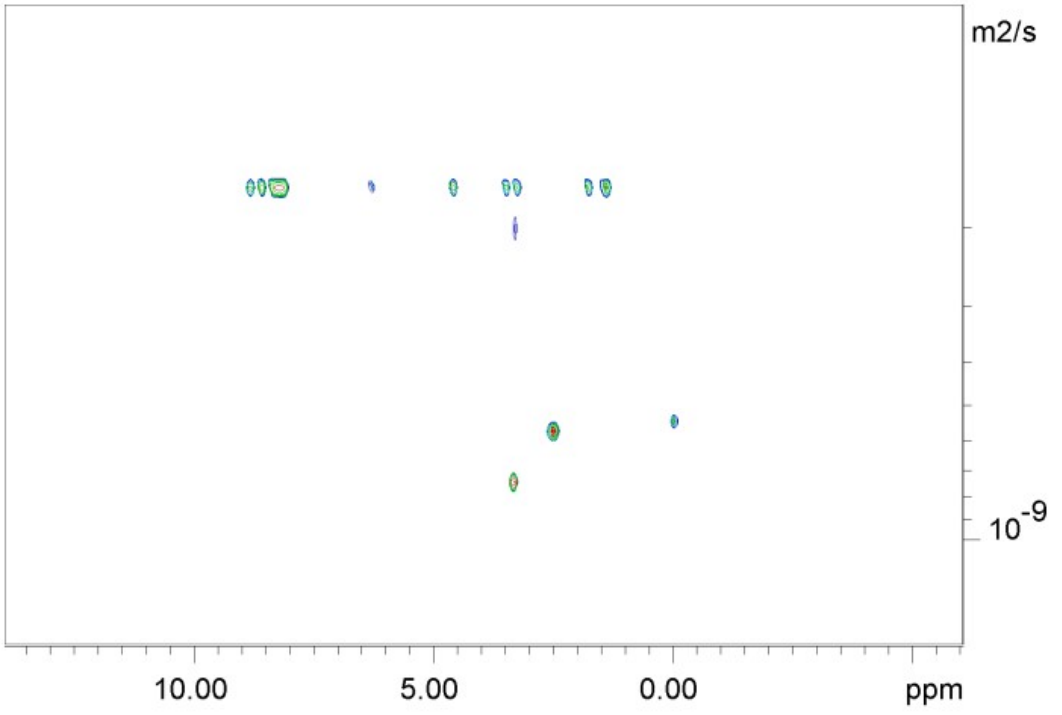

Figure S53. DOSY NMR spectra of ^{L}PMA in DMSO-d_6 with 298.15 K.

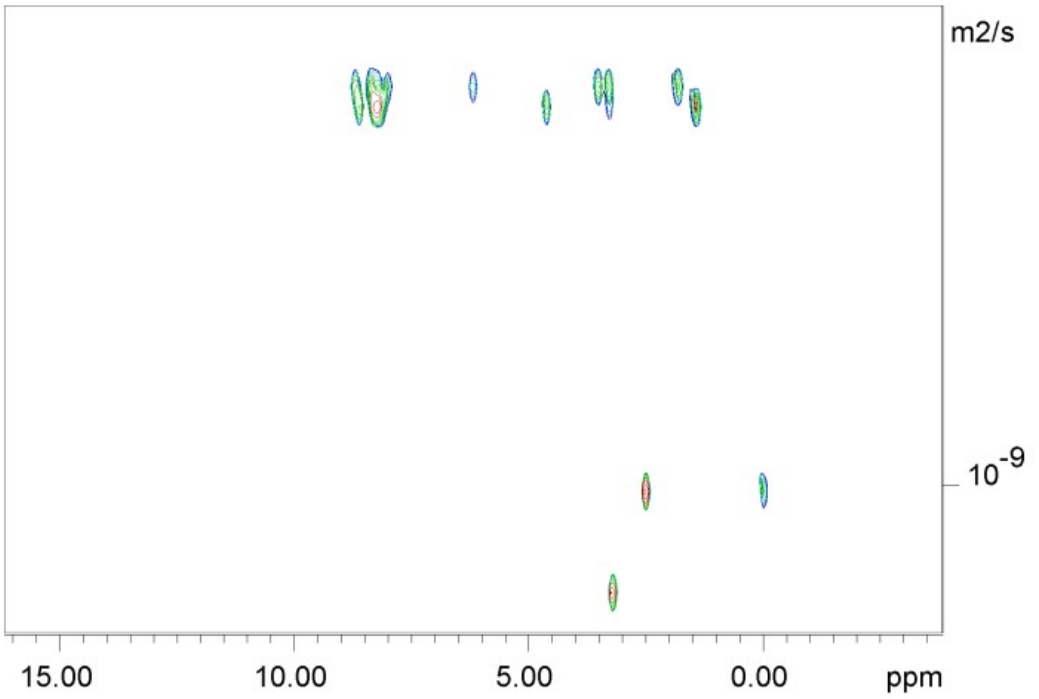

Figure S54. DOSY NMR spectra of ^{L}PMA in DMSO-d_6 with 323.15 K.

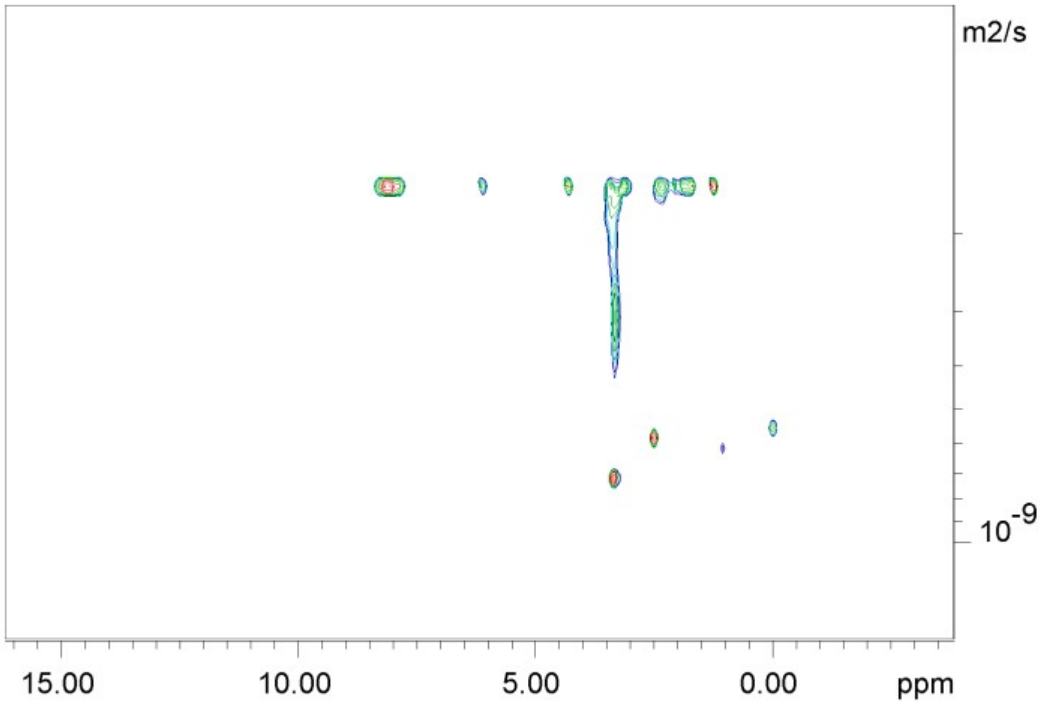

Figure S55. DOSY NMR spectra of ^{L}PBA in DMSO-d_6 with 298.15 K.

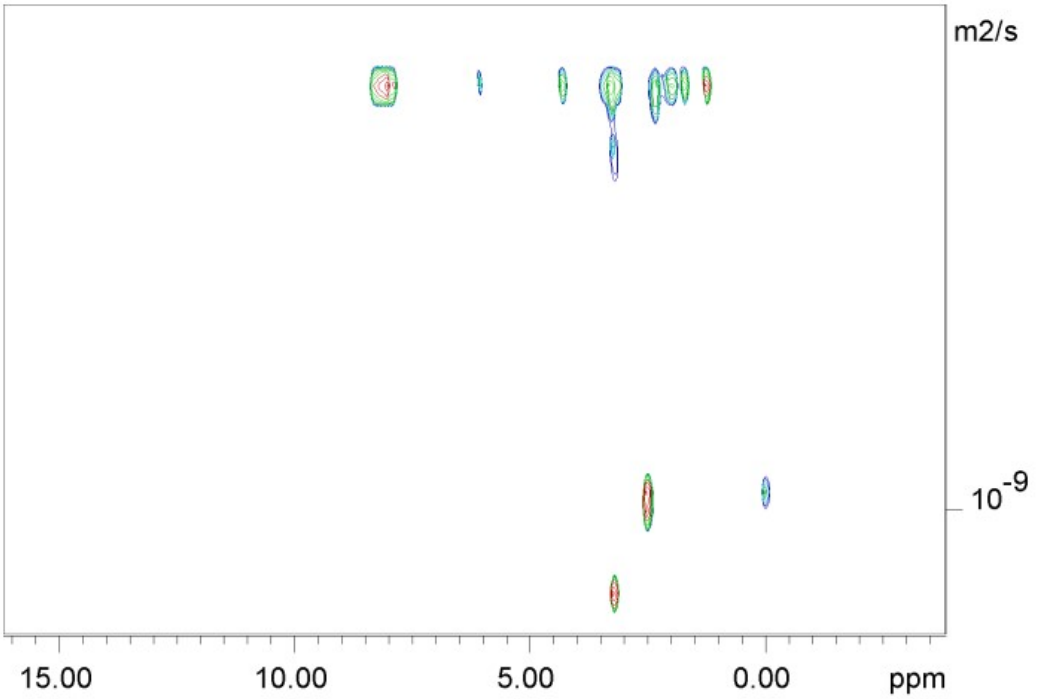

Figure S56. DOSY NMR spectra of ^{L}PBA in DMSO-d_6 with 323.15 K.

LPMA												
$CHCl_3$		K_B										
Oblate	b>a	p>1										
			log D									
D	1.04E-09		-8.982967									
T(K)	298.15											
η(Pa*s)	0.000536											
rh(sp)=kbT/6πDη		3.92E-10										
	b	a	rh(sp)	rh(ob)	fs	r(cal)	p	1/p	r(cal)/rh(ob	fs1	fs2	fs3
	5.50E-10	1.30E-10	3.92E-10	3.32E-10	1.18	3.40061E-10	4.23E+00	0.236	1.02E+00	4.111	2.616	1.332

Figure S57. Screenshot of Microsoft Excel spreadsheet used to fit ^{L}PMA in $CDCl_3$ with 298.15 K using oblate spheroid model.

LPMA										
$CHCl_3$		K_B								
Oblate	b>a	p>1								
			log D							
D	1.05E-10		-9.978811							
T(K)	318.15									
η(Pa*s)	0.000494									
rh(sp)=kbT/6πDη		4.49E-09								
	b	a	rh(sp)	rh(ob)	fs	r(cal)	p	1/p	r(cal)/rh(ob	f
	7.00E-10	3.00E-11	4.49E-09	2.40E-09	1.868	2.44966E-10	2.33E+01	0.043	1.02E-01	

Figure S58. Screenshot of Microsoft Excel spreadsheet used to fit ^{L}PMA in $CDCl_3$ with 318.15 K using oblate spheroid model.

LPBA									
$CHCl_3$		K_B							
Oblate	b>a	p>1							
			log D						
D	6.91E-10		-9.160522						
T(K)	298.15								
η(Pa*s)	0.000536								
rh(sp)=kbT/6πDη		5.90E-10							
	b	a	rh(sp)	rh(ob)	fs	r(cal)	p	1/p	r(cal)/rh(ob
	8.00E-10	2.50E-10	5.90E-10	5.28E-10	1.117	5.42884E-10	3.20E+00	0.313	1.03E+00

Figure S59. Screenshot of Microsoft Excel spreadsheet used to fit ^{L}PBA in $CDCl_3$ with 298.15 K using oblate spheroid model.

PBA									
$CHCl_3$		K_B							
Oblate	b>a	p>1							
			log D						
D	9.74E-10		-9.01144						
T(K)	318.15								
η(Pa*s)	0.000494								
rh(sp)=kbT/6πDη		4.84E-10							
	b	a	rh(sp)	rh(ob)	fs	r(cal)	p	1/p	r(cal)/rh(ob
	5.70E-10	3.30E-10	4.84E-10	4.72E-10	1.026162	4.75067E-10	1.73E+00	0.578947	1.006529

Figure S60. Screenshot of Microsoft Excel spreadsheet used to fit ^{L}PBA in $CDCl_3$ with 318.15 K using oblate spheroid model.

LPMA												
DMSO		K_B										
Oblate	b>a	p>1										
			log D									
D	1.61E-10		-9.793174									
T(K)	298.15											
η(Pa*s)	0.001967											
rh(sp)=kbT/6πDη		6.90E-10										
	b	a	rh(sp)	rh(ob)	fs	r(cal)	p	1/p	r(cal)/rh(ob	fs1	fs2	fs3
	8.90E-10	3.00E-10	6.90E-10	6.25E-10	1.103	6.19394E-10	2.97E+00	0.337	9.90E-01	2.793	2.065	1.227

Figure S61. Screenshot of Microsoft Excel spreadsheet used to fit ^{L}PMA in DMSO-d_6 with 298.15 K using oblate spheroid model.

LPMA									
DMSO		K_B							
Oblate	b>a	p>1							
			log D						
D	3.10E-10		-9.508638						
T(K)	323.15								
η(Pa*s)	0.001269								
rh(sp)=kbT/6πDη		6.02E-10							
	b	a	rh(sp)	rh(ob)	fs	r(cal)	p	1/p	r(cal)/rh(ob
	8.50E-10	2.80E-10	6.02E-10	5.44E-10	1.107	5.87037E-10	3.04E+00	0.329	1.08E+00

Figure S62. Screenshot of Microsoft Excel spreadsheet used to fit ^{L}PMA in DMSO-d_6 with 323.15 K using oblate spheroid model.

LPBA									
DMSO		K_B							
Oblate	b>a	p>1							
			log D						
D	1.57E-10		-9.8041						
T(K)	298.15								
η(Pa*s)	0.001967								
rh(sp)=kbT/6πDη		7.07E-10							
	b	a	rh(sp)	rh(ob)	fs	r(cal)	p	1/p	r(cal)/rh(ob)
	8.20E-10	4.90E-10	7.07E-10	6.91E-10	1.023	6.90676E-10	1.67E+00	0.598	9.99E-01

Figure S63. Screenshot of Microsoft Excel spreadsheet used to fit ^{L}PBA in DMSO-d_6 with 298.15 K using oblate spheroid model.

LPBA									
DMSO		K_B							
Oblate	b>a	p>1							
			log D						
D	2.84E-10		-9.546682						
T(K)	323.15								
η(Pa*s)	0.001269								
rh(sp)=kbT/6πDη		6.57E-10							
	b	a	rh(sp)	rh(ob)	fs	r(cal)	p	1/p	r(cal)/rh(ob)
	8.70E-10	2.90E-10	6.57E-10	5.95E-10	1.105	6.03224E-10	3.00E+00	0.333	1.01E+00

Figure S64. Screenshot of Microsoft Excel spreadsheet used to fit ^{L}PBA in DMSO-d_6 with 323.15 K using oblate spheroid model.

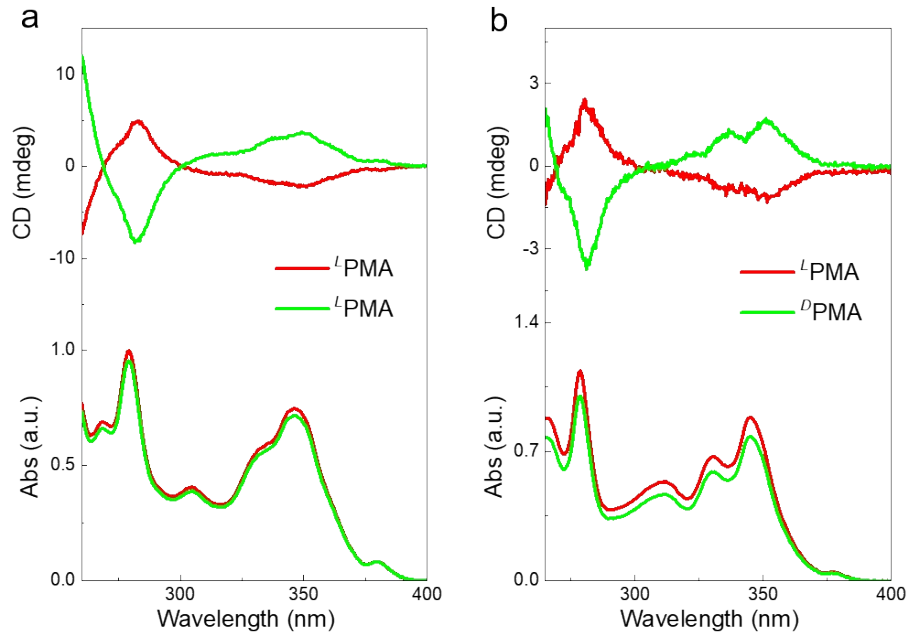

Figure S65. CD and corresponding UV-Vis absorption spectra of PMA in a) $CHCl_3$ and b) DMSO (0.3 mM).

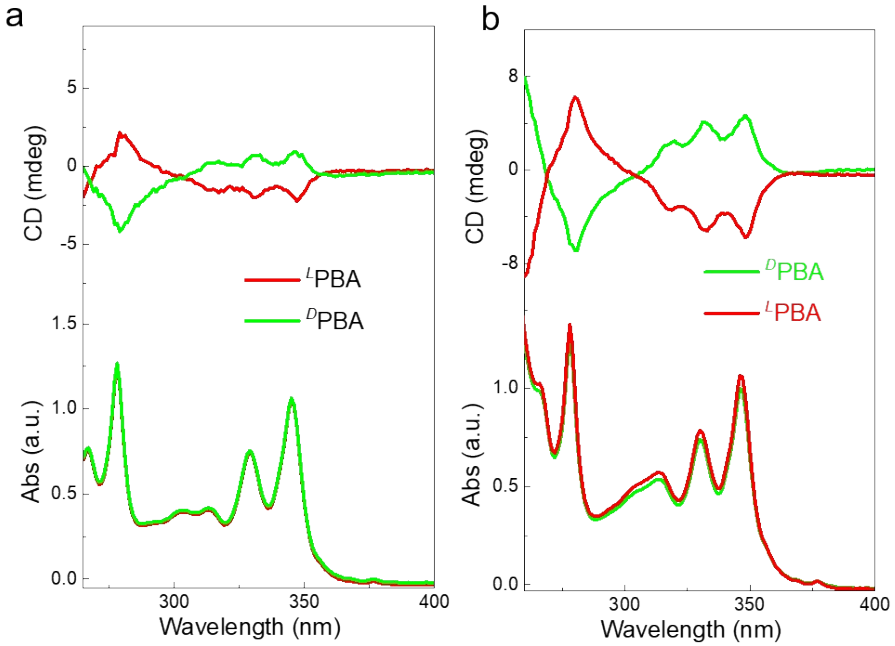

Figure S66. CD and corresponding UV-Vis absorption spectra of PBA in a) $CHCl_3$ and b) DMSO (0.3 mM)

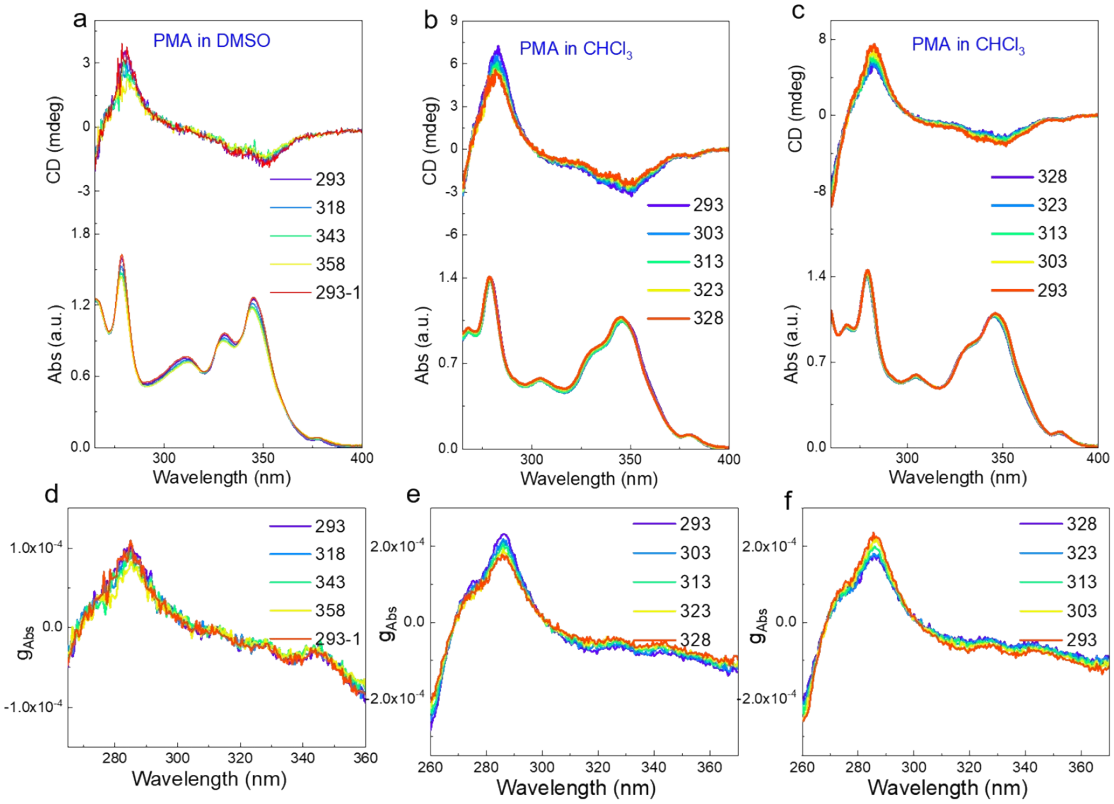

Figure S67. Temperature-variable CD spectra of ^{L}PMA and corresponding g_{Abs} (0.4 mM) in (a, d) DMSO and (b, e, c, f) $CHCl_3$ (g_{Abs} = CD/ Abs*32980)

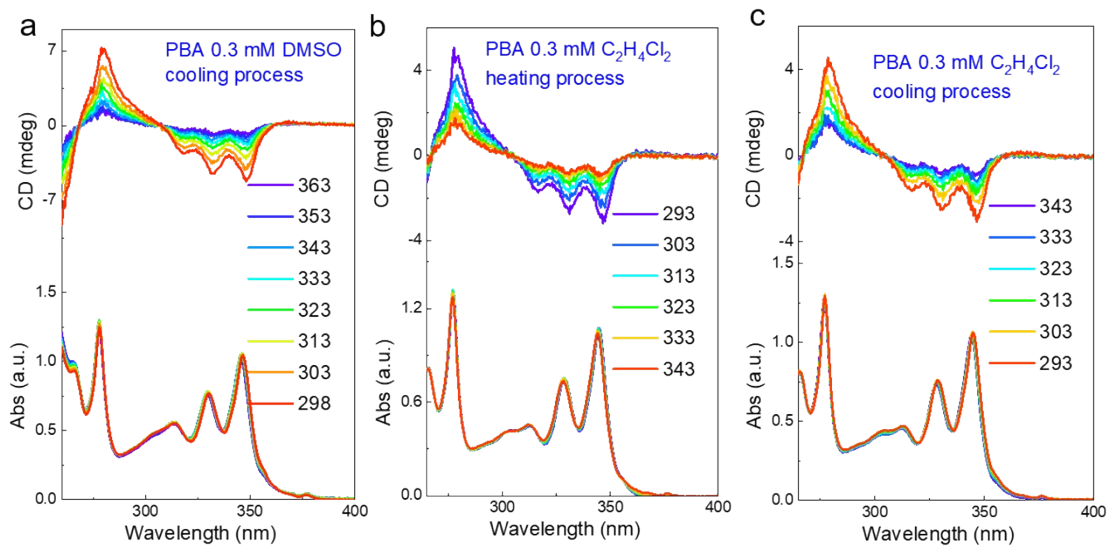

Figure S68. Temperature-variable CD spectra of ^{L}PBA (0.3 mM) in (a) DMSO and (b, c) $C_2H_4Cl_2$

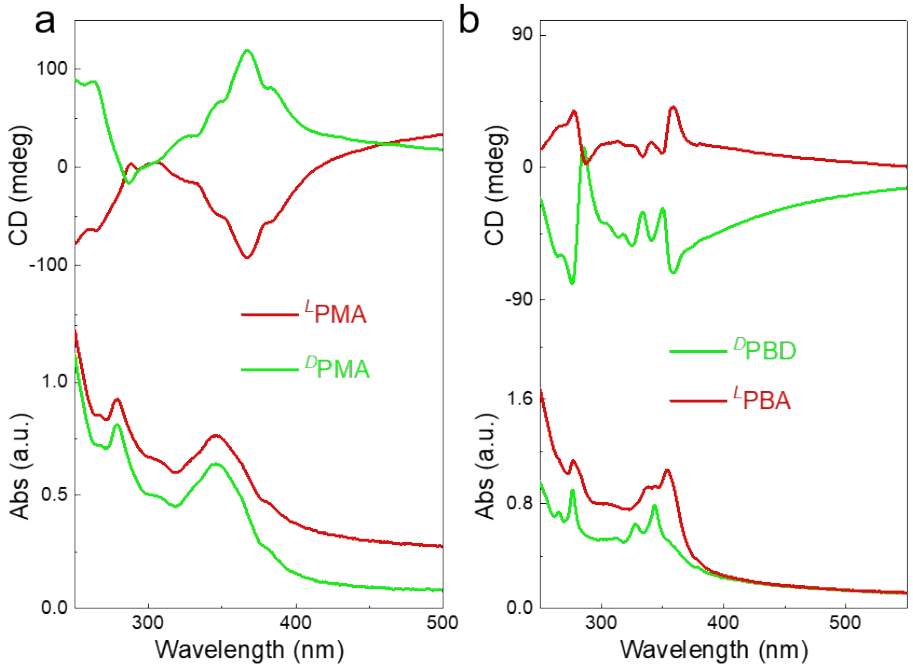

Figure S69. CD and corresponding UV-Vis absorption spectra of (a) PMA and (b) PBA in $CHCl_3$/MCH (2/8 by volume, 1 mM)

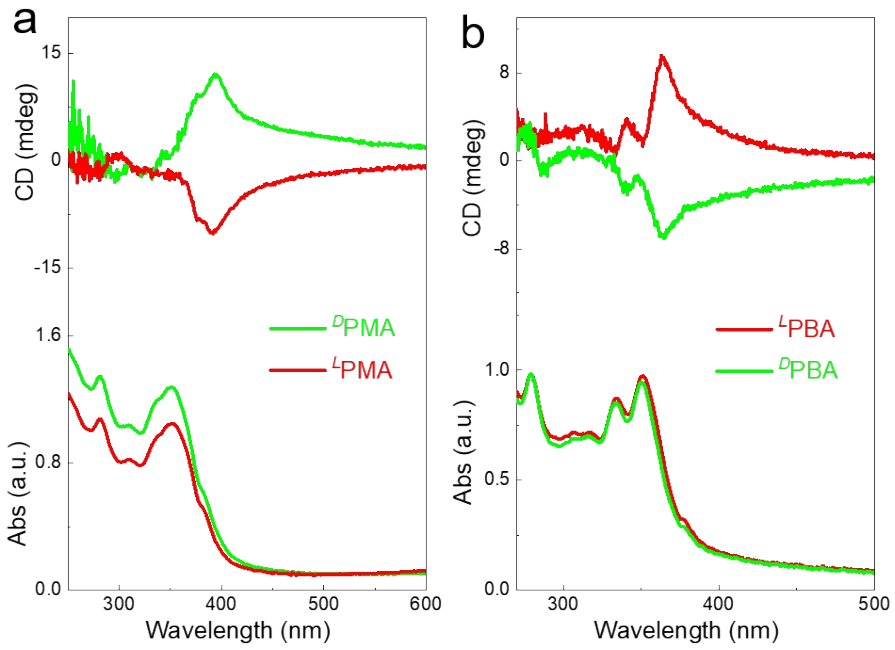

Figure S70. CD and corresponding UV-Vis absorption spectra of PMA and PBA crystals (1.8 mg solid with 540 mg KBr)

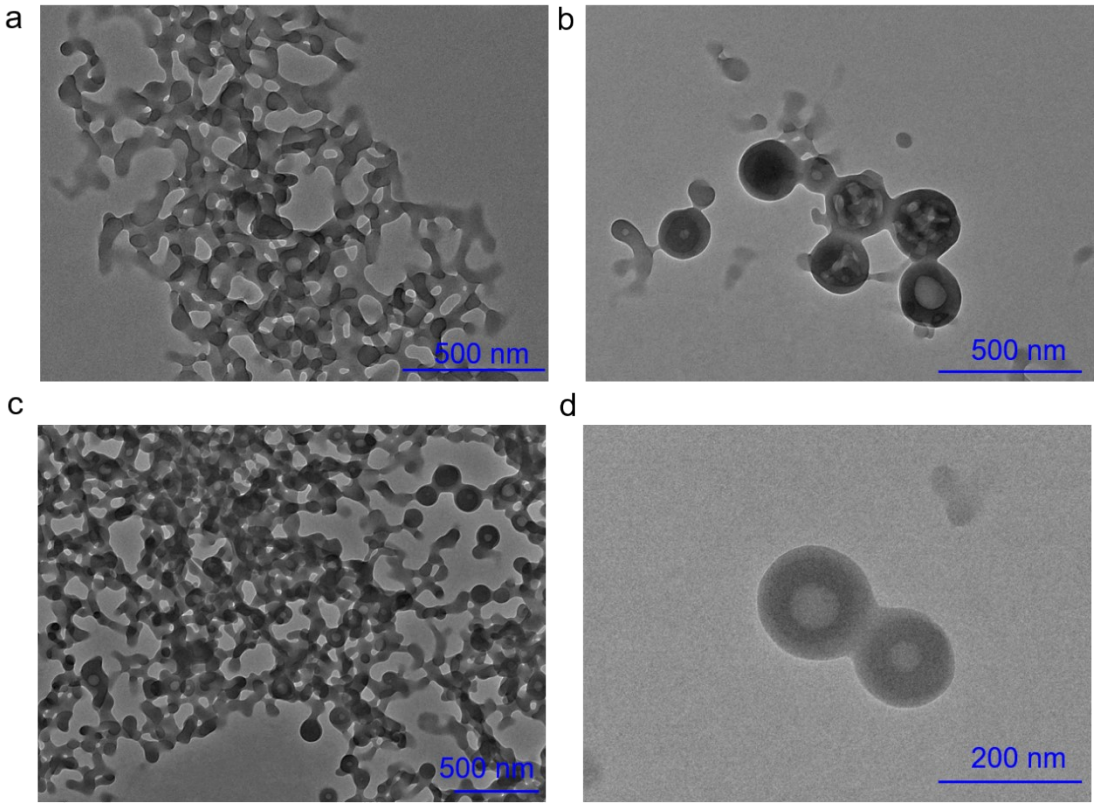

Figure S71. TEM images of self-assembled ^{L}PMA and ^{L}PBA in the mixture of DMSO/H_2O (30/970 by volume, 1 mM).

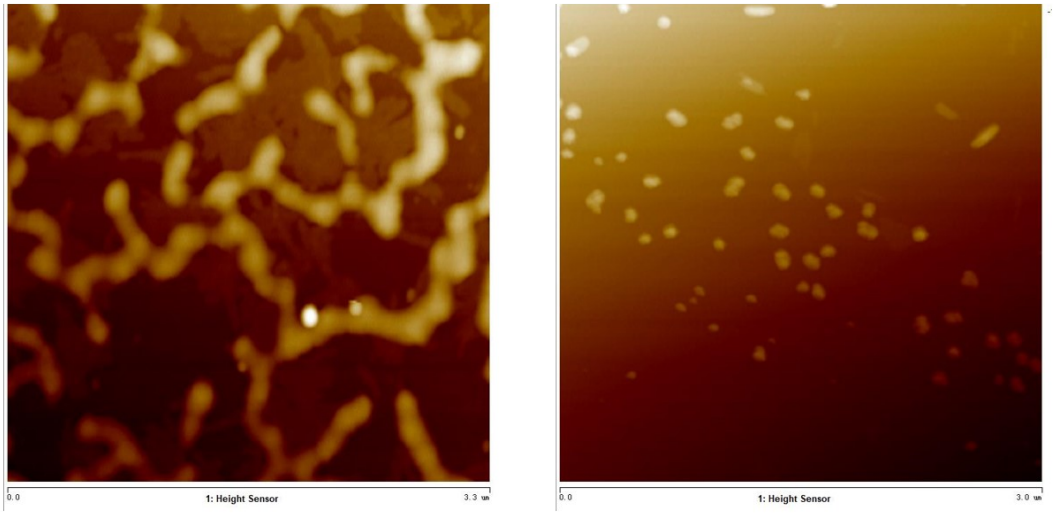

Figure S72. AFM images of self-assembled ^{L}PMA and ^{L}PBA in the mixture of DMSO/H_2O (30/970 by volume, 1 mM).

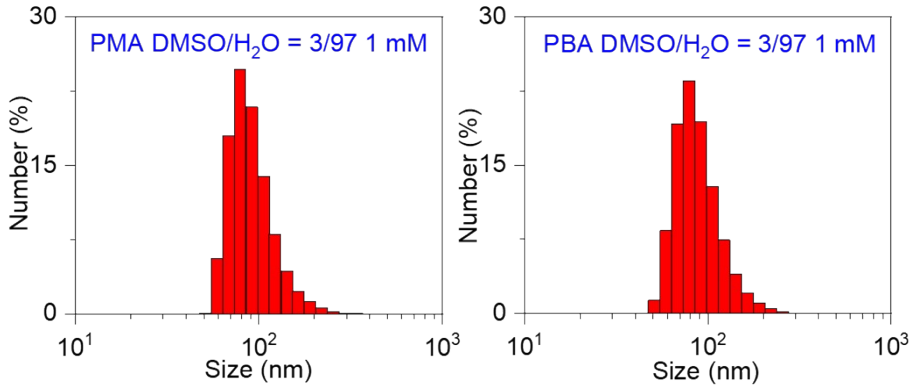

Figure S73. DLS of self-assembled ^{L}PMA and ^{L}PBA in the mixture of DMSO/H_2O (30/970 by volume, 1 mM)

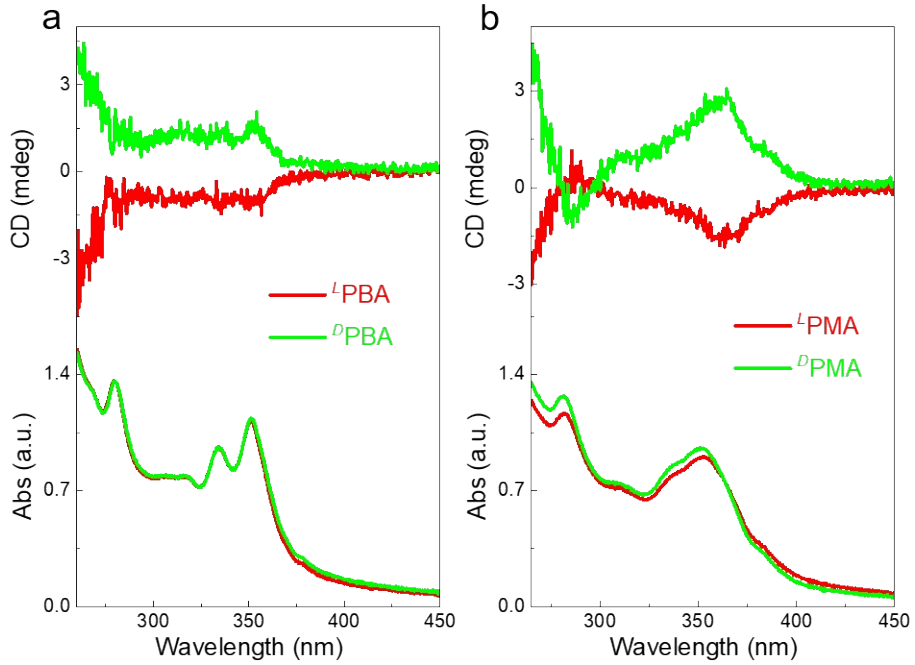

Figure S74. CD and corresponding UV-Vis absorption spectra of PMA and PBA assemblies in DMSO/H_2O (30/970 by volume, 1 mM).

References

(1) Lu, T.; Chen, F. Multiwfn: A Multifunctional Wavefunction Analyzer, *J. Comput. Chem*. **2012**, *33,* 580-592.

(2) Johnson, E. R.; Keinan, S.; Mori-Sánchez, P.; Contreras-García, J.; Cohen, A. J.; Yang, W. Revealing Noncovalent interactions. *J. Am. Chem. Soc*. **2010**, *132*, 6498-6506.

(3) Gaussian 16, Revision A.03, Frisch, M. J.; Trucks, G. W.; Schlegel, H. B.; Scuseria, G. E.; Robb, M. A.; Cheeseman, J. R.; Scalmani, G.; Barone, V.; Petersson, G. A.; Nakatsuji, H.; Li, X.; Caricato, M.; Marenich, A. V.; Bloino, J.; Janesko, B. G.; Gomperts, R.; Mennucci, B.; Hratchian, H. P.; Ortiz, J. V.; Izmaylov, A. F.; Sonnenberg, J. L.; Williams-Young, D.; Ding, F.; Lipparini, F.; Egidi, F.; Goings, J.; Peng, B.; Petrone, A.; Henderson, T.; Ranasinghe, D.; Zakrzewski, V. G.; Gao, J.; Rega, N.; Zheng, G.; Liang, W.; Hada, M.; Ehara, M.; Toyota, K.; Fukuda, R.; Hasegawa, J.; Ishida, M.; Nakajima, T.; Honda, Y.; Kitao, O.; Nakai, H.; Vreven, T.; Throssell, K.; Montgomery, J. A.; Peralta, J. E.; Ogliaro, F.; Bearpark, M. J.; Heyd, J. J.; Brothers, E. N.; Kudin, K. N.; Staroverov, V. N.; Keith, T. A.; Kobayashi, R.; Normand, J.;

Raghavachari, K.; Rendell, A. P.; Burant, J. C.; Iyengar, S. S.; Tomasi, J.; Cossi, M.; Millam, J. M.; Klene, M.; Adamo, C.; Cammi, R.; Ochterski, J. W.; Martin, R. L.; Morokuma, K.; Farkas, O.; Foresman, J. B.; Fox, D. J. Gaussian, Inc., Wallingford CT, **2016**.

(4) Spackman, P. R.; Turner, M. J.; McKinnon, J. J.; Wolff, S. K.; Grimwood, D. J.; Spackman, D, J, M. A, CrystalExplorer: a Program for Hirshfeld Surface Analysis, Visualization and Quantitative Analysis Of Molecular Crystals. *J. Appl. Cryst.* **2021**, *54*, 1006-1011.

(5) Avram, L.; Cohen, Y. Diffusion NMR of Molecular Cages and Capsules. *Chem. Soc. Rev.* **2015**, *44*, 586-602.

(6) Zhang, Z.; Wang, H.; Wang, X.; Li, Y.; Song, B.; Bolarinwa, O.; Reese, R. A.; Zhang, T.; Wang, X.; Cai, J.; Xu, B.; Wang, M.; Liu, C.; Yang, H.; Li, X. Supersnowflakes: Stepwise Self-Assembly and Dynamic Exchange of Rhombus Star-Shaped Supramolecules. *J. Am. Chem. Soc*. **2017**, *139*, 8174-8185.

(7) Giuseppone, N. Schmitt, J.-L.; Allouche, L.; Lehn, J. M. DOSY NMR Experiments as a Tool for the Analysis of Constitutional and Motional Dynamic Processes: Implementation for the Driven Evolution of Dynamic Combinatorial Libraries of Helical Strands. *Angew. Chem. Int. Ed.* **2008**, *47*, 2235-2239.

(8) Schulze, B. M.; Watkins, D. L.; Zhang, J.; Ghiviriga, I.; Castellano, R. K. Estimating the shape and Size of Supramolecular Assemblies by Variable Temperature Diffusion Ordered Spectroscopy. *Org. Biomol. Chem*. **2014**, *12*, 7932-7936.

(9) https://wiki.anton-paar.com/en/chloroform/.